J. Fluid Mech. (2009), *vol.* 633, *pp.* 233–269.
doi:10.1017/S0022112009007472 Printed in the United Kingdom

The dynamics and rheology of a dilute suspension of hydrodynamically Janus spheres in a linear flow

ARUN RAMACHANDRAN AND ADITYA S. KHAIR†

Department of Chemical Engineering, University of California, Santa Barbara, CA 93106-5080, USA

(Received 24 June 2008 and in revised form 12 March 2009)

The creeping motion of a hydrodynamically 'Janus' spherical particle, whose surface is partitioned into two distinct regions, is investigated. On one region, fluid adjacent to the particle obeys the no-slip condition, whereas on the other, fluid slips past the particle. The fore-aft asymmetry of this 'slip–stick' sphere (Swan & Khair, *J. Fluid Mech.*, vol. 606, 2008, p. 115) leads to a number of interesting results when it is placed in different flows, which is illustrated by computing the particle motion to first order in the ratio of slip length to particle radius. For example, in a pure straining field the sphere attains an equilibrium orientation either along the compressional or extensional axis of the flow, depending on the ratio of slip-to-stick surface areas. In a simple shear flow, on the other hand, the slip–stick sphere undergoes a periodic rotational motion, or Jeffrey orbit. Moreover, depending on its initial orientation, the particle can either follow a periodic translational orbit or undergo a net displacement along the flow direction. Lastly, to first order in the volume fraction of slip–stick spheres, the suspension rheology is non-Newtonian, with non-zero first and second normal stress differences.

1. Introduction

The last decade has witnessed spectacular progress in the fabrication of nanoscale colloidal particles with anisotropic shapes and surface properties (Glotzer & Solomon 2007). Recent reviews by Perro *et al.* (2005) and Walther & Muller (2008) have focused on a particularly fascinating subset of these particles known as 'Janus' spheres – named after the double-headed Roman god – which possess two 'faces' that can be designed to be chemically (Roh, Martin & Lahann 2005; Hong, Jian & Granick 2006; Nie *et al.* 2006), electrically (Takei & Shimizu 1997; Cayre, Paunov & Velev 2003) or magnetically (Velev, Lenhoff & Kaler 2000) distinct. The potential applications of Janus particles are wide ranging and include switchable display devices (Nisisako *et al.* 2006), micro-rheological probes (Behrend *et al.* 2005) and emulsification agents (Casagrande *et al.* 1989; Glaser *et al.* 2006). Furthermore, the dual-faced nature of a Janus particle can lead to directed motion in the presence of an applied field, which may be of interest in the context of microfluidics. For example, Gangwal *et al.* (2008) fabricated 'metallodielectric' Janus microspheres with one dielectric and one metal-coated hemisphere. When suspended in an aqueous electrolyte, application of an AC electric field causes such a particle to steadily translate perpendicular

† Email address for correspondence: akhair@engineering.uscb.edu

to the field via induced-charge electrophoresis, in agreement with the theoretical predictions of Squires & Bazant (2006). Moreover, Janus particles can be designed to create localized gradients and therefore move autonomously. On this note, Howse *et al.* (2007) constructed a microscale Janus swimmer consisting of a polystyrene sphere with one platinum-coated hemisphere. The platinum acts as a catalyst for the reduction of hydrogen peroxide (the 'fuel'); the resulting asymmetric distribution of reaction products generates a local gradient in osmotic pressure that propels the microswimmer. In this paper, we consider theoretically a Janus particle whose two faces are distinct from a hydrodynamic viewpoint, such that on one face fluid adjacent to the particle satisfies the no-slip condition, whereas on the other, fluid slips past the particle. Before venturing into the specifics of the present work, however, we briefly review some fundamental aspects of slip at fluid–solid interfaces.

For a solid surface, the most commonly used boundary condition for the velocity field is the no-slip (or stick) condition, which states that the velocity of a fluid element adjacent to a surface is equal to the velocity of the surface. It is important, however, to note that the no-slip boundary condition is an assumption that cannot be proved rigorously. Indeed, the classic monographs of Lamb (1932) and Batchelor (1973) state that while the no-slip condition is, in most cases, obeyed, there may exist certain situations in which slip does occur. In a recent review, Lauga, Brenner & Stone (2007) discussed two general mechanisms that may cause slip. The first is molecular or intrinsic slip, wherein individual fluid molecules move relative to a solid surface through the action of hydrodynamic (shear) forces. The second mechanism is that of effective or apparent slip. Here, microscopic inhomogeneities at a fluid–solid interface give rise to an effective slip at the macroscopic scale.

Approximately 200 years ago, Navier (1823) proposed a phenomenological boundary condition that remains to this day the simplest and most commonly used model for slip at fluid–solid boundaries. The so-called 'Navier slip condition' states that the tangential velocity of a fluid element relative to a solid surface is proportional to the rate of strain of the element. The scalar constant of proportionality is known as the slip length λ. Mathematically, the Navier slip condition can be written as

$$u_i - U_i = 2\lambda(\delta_{ij} - n_i n_j)E_{jk}n_k, \tag{1.1}$$

where u_i and U_i are the velocity of the fluid and solid surfaces, respectively; n_i is the unit normal vector pointing into the fluid; δ_{ij} is the identity tensor; and $E_{ij} = (1/2)(\partial u_i/\partial x_j + \partial u_j/\partial x_i)$ is the rate of strain tensor with x_i as the position vector. The slip velocity is simply the difference between the fluid and surface velocities, $u_i - U_i$. Clearly, if $\lambda = 0$ one recovers the no-slip condition; at the opposite extreme, as $\lambda \to \infty$, the tangential strain at the surface vanishes. Note that while the Navier slip condition allows for a non-zero tangential slip velocity, the relative velocity normal to the fluid–solid interface, $n_i(u_i - U_i)$, must equal zero as fluid cannot pass through the surface. Importantly, in (1.1) the slip length λ is assumed to be independent of the shear rate $\dot{\gamma} = \sqrt{2E_{ij}E_{ji}}$, with the consequence that the Navier boundary condition is linear in the fluid velocity. Molecular Dynamics simulations of simple shear flow between parallel plates by Thompson & Troian (1997) verified that the Navier slip condition is valid for sufficiently low shear rates; at higher shear rates, however, λ is found to grow in a nonlinear manner with $\dot{\gamma}$.

A simple example of the effect of slip is provided by considering pressure-driven flow through a circular channel of radius a. If fluid does not slip at the channel walls one recovers the classic Hägen–Poiseuille velocity profile, and the flow rate through the channel is given by $Q = (\pi a^4/8\mu_0)\Delta P$, where μ_0 is the viscosity and

ΔP is the applied pressure gradient. If the channel exhibits slip, however, a slip flow proportional to the shear rate at the wall is generated, and the ratio of slip to no-slip flow rates is $Q_{slip}/Q = 1 + 4\lambda/a$. The above example is, in fact, used as the basis for measuring slip lengths experimentally (Cheng & Giordano 2002; Choi *et al.* 2003). In this technique it is assumed, by construction, that the Navier slip condition applies throughout the domain of interest. However, in a micro-fabricated channel, for example, one expects some degree of heterogeneity as a consequence of the manufacturing process or via contamination of the walls by molecules in the surrounding fluid. For example, it has been postulated (Lauga & Stone 2003) that the large values of slip length measured for pressure-driven flow of water through hydrophobically coated capillaries is due to nucleation of 'nano-bubbles' at the walls (Tyrrell & Attard 2001); the nano-bubbles act as zero shear stress (infinite slip length) patches. Thus, it is possible that the local slip length may vary with position along a channel. What is actually being measured in a pressure drop versus flow rate experiment, then, is an effective slip length averaged across a portion of the channel (Lauga *et al.* 2007). This issue was addressed by Lauga & Stone (2003) (see also Philip 1972*a*, *b*), who computed the effective slip length for pressure-driven flow through a cylindrical channel whose surface is patterned, either parallel or transverse to the pressure gradient, into alternating regions of no-slip ($\lambda = 0$) and no shear ($\lambda \to \infty$). Similarly, Priezjev, Darhuber & Troian (2005) compared the velocity fields and effective slip length from Molecular Dynamics simulations to solution of the Stokes equations for a parallel plate geometry in which the top plate translates at constant velocity while the stationary bottom plate is patterned into periodic strips of perfect slip and finite slip. When the strip widths are greater than 10 fluid molecular diameters each, the two methods are in excellent agreement. For smaller strip widths, the bottom plate appears molecularly rough, and the effective slip length computed from Molecular Dynamics simulations is lesser than that from the Stokes equations.

One can also consider the effects of slip on the motion of particles in a viscous fluid. For instance, Basset (1961) examined an isotropically slipping sphere of radius a under the action of an applied force F_i at low Reynolds numbers. The velocity acquired by the sphere U_i is equal to

$$U_i = \left(\frac{1 + 3\lambda/a}{1 + 2\lambda/a}\right) \frac{F_i}{6\pi\mu_0 a}. \tag{1.2}$$

For a no-slip sphere ($\lambda = 0$), one recovers the Stokes drag, $U_i = F_i/6\pi\mu_0 a$. As λ increases the shear stress on the particle surface diminishes, causing the velocity to increase. Ultimately, as $\lambda/a \to \infty$ one finds $U_i = F_i/4\pi\mu_0 a$, which is also equal to the velocity of a translating spherical bubble. This is unsurprising as the boundary conditions on the surface of a bubble – no relative normal velocity and zero tangential stress – are the same as those for a perfectly slipping sphere. Note that as the slip length is uniform over the sphere's surface, the mobility of the particle is isotropic; that is, the sphere translates solely in the direction of the applied force.

From the above discussion, a question that naturally arises is: what is the velocity of the sphere when the slip length is not uniform over its surface? Swan & Khair (2008) have addressed this question by analysing a simple model system for a hydrodynamically Janus particle – the 'slip–stick' sphere, whose surface is partitioned into two distinct regions. Over one region, fluid obeys the no-slip condition and over the other, fluid slips according to the Navier boundary condition (see figure 1). In the small-slip-length limit $\lambda/a \ll 1$, they derived Faxén-type laws relating the translational and rotational motions of a slip–stick sphere to the various moments of force density

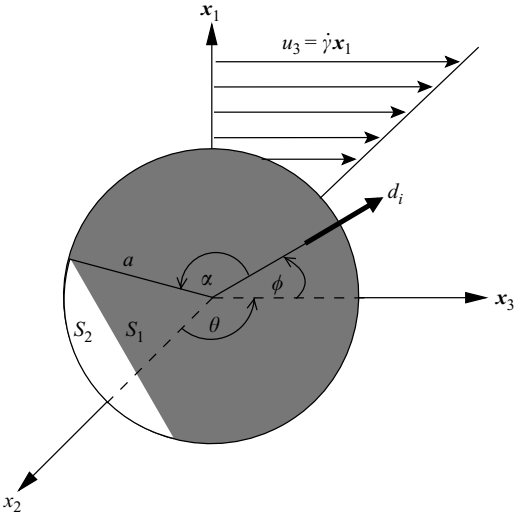

FIGURE 1. Definition sketch for a hydrodynamically Janus slip–stick sphere of radius a in a linear flow. Fluid slips over the surface S_1 whereas the no-slip condition is obeyed on surface S_2; the relative surface areas of S_1 and S_2 are set by the 'slipping' angle α. The slip–stick asymmetry is characterized by the director d_i, which is a unit vector perpendicular to the slip–stick dividing plane and pointing into the slip side S_1. The orientation of d_i with respect to a right-handed Cartesian coordinate system is given by two angles: (i) equatorial angle ϕ measuring the angle between the director and the x_3 axis; and (ii) polar angle θ measuring the angle between d_i and the x_2 axis. In the sketch a representative shear flow $u_3 = \dot{\gamma} x_1$ (with $\dot{\gamma}$ the shear rate) in the x_3–x_1 (velocity–velocity gradient) plane is shown.

on its surface. For example, application of a force F_i on a slip–stick sphere causes it to translate with a velocity U_i given by (see appendix C)

$$U_i = \left(1 + \frac{\lambda}{8a}\left[(4 - \cos^3\alpha - 3\cos\alpha)\delta_{ij} - 3\cos\alpha\sin^2\alpha\, d_i d_j\right]\right)\frac{F_j}{6\pi\mu_0 a} + O(\lambda/a)^2, \tag{1.3}$$

where α is the dividing or slipping angle demarcating the slip and no-slip parts of the surface (see figure 1), and d_i denotes the symmetry axis, or director, of the particle. Clearly, if $\alpha = 0$ the entire surface is no-slip and we recover Stokes drag; for $\alpha = \pi$ the entire surface (slightly) slips and $U_i = (1 + \lambda/a)F_i/6\pi\mu_0 a$ in agreement with (1.2) for $\lambda/a \ll 1$. More interestingly, for intermediate values of α, the mobility of the sphere is no longer isotropic (except for the special case of a half-slipping sphere $\alpha = \pi/2$); that is, generally, the slip–stick sphere does not translate solely in the direction of the applied force. The key point is that the Janus nature of the sphere's surface dictates that while the particle is geometrically spherical, it is no longer spherically symmetric from a hydrodynamic viewpoint. The slip–stick sphere is a body of revolution, nonetheless, and in analogy with other axisymmetric bodies in Stokes flow (e.g. a spheroid), the resistances to motion parallel and perpendicular to the symmetry axis are, in general, different.

We would like to emphasize here that hydrodynamically Janus particles may actually be observed in a variety of physical settings. It was shown by Boehnke *et al.* (1999) that a non-neutrally buoyant hydrophobic micron-sized particle when immersed in a polar suspending fluid settles with a velocity that is about 20 %

greater than that predicted by Stokes drag. This increase in the settling speed was attributed to the presence of nanometre-sized air bubbles attached to the surface of the sphere. The bubbles serve as zero shear stress regions for the suspending fluid, and Boehnke *et al.* (1999) ascribed to the surface an isotropic effective slip length of $\lambda/a = 0.5$. By analogy, an amphiphilic Janus sphere – such as made by Casagrande *et al.* (1989) – when immersed in a polar liquid should also have nano-bubbles attached to its hydrophobic hemisphere, thus endowing that face with an effective slip length. On the other hand, the hydrophilic hemisphere should be a bubble-free no-slip boundary. Particles with surfaces partitioned into slip and no-slip regions may also be encountered in other physical situations. For example, vesicles synthesized from a mixture of two different double-chain surfactants typically display 'solid' and 'fluid' domains at temperatures intermediate to the phase transition temperatures of the two components (Korlach *et al.* 1999; Dietrich *et al.* 2001). Another simple example is the creeping flow of fluid over a bubble or a drop with a stagnant cap. It is well known from experiments that a rising bubble or drop accumulates surfactant at its downstream end (Beitel & Heidger 1971; Sadhal & Johnson 1983). In the limit of small surface diffusivities, the surfactant is tightly packed into a cap and fluid obeys the no-slip boundary condition over the cap. The remainder of the surface is surfactant free and therefore mobile. One can also envisage the synthesis of a slip–stick sphere by fusing an impermeable hemisphere and a porous hemisphere. When placed in solution air would cover the surfaces of the pores thereby creating a collection of no-shear (i.e. perfect slip) zones over the porous portion of the sphere. Thus, one could ascribe to the porous hemisphere an effective slip length (e.g. Taylor 1971). (We are grateful to Dr D. T. Leighton for this suggestion.)

In this paper, we consider the motion of a force- and torque-free slip–stick sphere immersed in a linear flow at low Reynolds numbers. Using linearity arguments we demonstrate that a slip–stick sphere can translate and rotate relative to the linear flow. In particular, for a two-dimensional straining flow it is shown that a slip–stick sphere acquires an equilibrium orientation along either the extensional or compressional axis of the flow, whereas in a simple shear flow the sphere undergoes a periodic rotational motion, or Jeffrey orbit. Moreover, depending on the initial orientation of the director with respect to the shear flow, the slip–stick sphere may either execute a periodic translational orbit or undergo a net displacement in the flow direction. The rheology of a dilute suspension of slip–stick spheres is found to be equally rich; even to first order in the particle volume fraction the suspension is non-Newtonian, with non-zero first and second normal stress differences.

The present work is similar in spirit to that of Nir & Acrivos (1973) who studied the motion of a freely suspended aggregate, or doublet, consisting of two unequal touching spheres in a linear flow. (Note, the no-slip condition is obeyed on the surface of each sphere). The aggregate constitutes an axisymmetric fore-aft asymmetric body; hence, just as for a slip–stick sphere, the doublet migrates in a simple shear flow and undergoes periodic rotational motion. Moreover, a suspension of such aggregates possesses a non-Newtonian rheology to first order in the doublet volume fraction. On a related theme, Dorrepaal (1978) considered the dynamics of a spherical cap in a simple shear flow. Once again, the spherical cap is a fore-aft asymmetric body of revolution that translates in a shear flow while executing cyclical orientational motion.

In § 2 we present governing equations for the slip–stick sphere in a linear flow. Furthermore, using the linearity of Stokes equations and the fact that a single vector d_i characterizes the slip–stick asymmetry we derive simple expressions for the

translational and angular velocities of the particle as a function of the imposed flow field. These expressions contain *a priori* unknown coefficients that are determined by an explicit solution of the Stokes equations via Lamb's solution in the limit $\lambda/a \ll 1$. In § 3 we consider the dynamics of a slip–stick sphere in a straining flow and simple shear. The rheological properties of dilute suspension of slip–stick spheres are discussed in § 4. Finally, in § 5, we draw some conclusions.

2. Governing equations and consequences of linearity

Consider a hydrodynamically Janus slip–stick sphere of radius a freely suspended in a linear flow. Under creeping flow conditions the velocity field in the fluid u_i obeys the Stokes equations

$$\mu_0 \frac{\partial^2 u_i}{\partial x_j \partial x_j} - \frac{\partial p}{\partial x_i} = 0, \quad \text{and} \quad \frac{\partial u_i}{\partial x_i} = 0, \tag{2.1}$$

where μ_0 is the viscosity of the suspending fluid, p is the pressure and x_i is the position vector measured from the centre of the particle. Far from the slip–stick particle, the fluid velocity approaches the imposed linear flow

$$u_i \to \epsilon_{ijk}\omega_j^\infty x_k + E_{ij}^\infty x_j, \quad \text{as} \quad r \to \infty, \tag{2.2}$$

where ϵ_{ijk} is the third-order unit alternating tensor and $r = (x_j x_j)^{1/2}$. In the above, E_{ij}^∞ and $2\omega_i^\infty$ are the rate of strain and vorticity of the undisturbed flow, respectively. Over the no-slip portion of the sphere S_2 (see figure 1), the fluid velocity satisfies

$$u_i = U_i + \epsilon_{ijk}\omega_j x_k, \tag{2.3}$$

where U_i and ω_i are the translational velocity and angular velocity of the particle, respectively. Note that U_i and ω_i are not specified *a priori*; instead they will be found from the requirement that the particle is force and torque free. On the hydrodynamically slipping part of the surface, S_1, the fluid velocity obeys the Navier boundary condition

$$u_i = U_i + \epsilon_{ijk}\omega_j x_k + 2\beta\left(\delta_{ij} - n_i n_j\right) E_{jk} x_k, \tag{2.4}$$

where n_i is the unit normal; $\beta = \lambda/a$ is the dimensionless slip length and E_{ij} is the local rate of strain.

The complicated (mixed) nature of the slip–stick boundary condition renders solution of the Stokes equations for the velocity and pressure fields a challenging task. However, one can exploit the linearity of the Stokes equations and the fact that the orientation of the particle is specified uniquely by the director, d_i, to derive simple expressions for the translational and angular velocities of the particle in terms of d_i and the ambient rate of strain E_{ij}^∞. Following Bretherton (1962) and Nir & Acrivos (1973), for a freely suspended sphere the difference between the angular velocity of the particle and that of the ambient flow is given by

$$\omega_i - \omega_i^\infty = \beta B(\alpha, \beta)\epsilon_{ijk} d_j d_m E_{km}^\infty, \tag{2.5}$$

where the scalar B is a function of the slip–stick dividing angle α and the non-dimensional slip length β only. Clearly, if the surface is either uniformly no-slip ($\alpha = 0$ or $\beta = 0$) or uniformly slip ($\alpha = \pi$), the particle is spherically symmetric and thus the sphere simply rotates with the ambient angular velocity ω_i^∞. For intermediate values of α and non-zero β, however, B is non-zero and must be found from an explicit

solution of the Stokes equations subject to the slip–stick boundary conditions and the requirement that the particle is force and torque free. Similar linearity arguments can be used to write the translational velocity as

$$U_i = a\beta \left[f_1(\alpha, \beta) E^{\infty}_{ij} d_j + f_2(\alpha, \beta) d_i d_j d_k E^{\infty}_{jk} \right], \tag{2.6}$$

where the functions f_1 and f_2 again vanish if $\alpha = 0$, $\alpha = \pi$ or $\beta = 0$.

Even though the above (exact) expressions for the rotational and translational velocities derived from linearity arguments appear simple, one can illustrate their power in the following example. Consider the sphere placed in the simple shear flow $u_3 = \dot{\gamma} x_1$ and oriented along the flow direction ($d_i = \delta_{i3}$). In this case,

$$\omega_1 - \omega_1^{\infty} = 0, \quad \omega_2 - \omega_2^{\infty} = -B(\alpha, \beta)\frac{\dot{\gamma}}{2}, \quad \omega_3 - \omega_3^{\infty} = 0, \tag{2.7}$$

so that deviation from the local rotational motion is along the vorticity axis only. On the other hand, the translational velocity becomes

$$U_1 = \lambda f_1(\alpha, \beta)\frac{\dot{\gamma}}{2}, \quad U_2 = 0, \quad U_3 = 0, \tag{2.8}$$

which implies that translation relative to the local flow occurs only along the velocity gradient axis.

Note that a fore–aft symmetric particle such as a prolate spheroid will not translate when placed at the centre of a linear flow. This is because such a particle is physically invariant to reflection about its equatorial plane of symmetry. The translational velocity should thus be unaffected by the transformation $d_i \to -d_i$, which is possible only when $f_1 = f_2 \equiv 0$. The slip–stick particle, on the other hand, is Janus and therefore not fore–aft symmetric; consequently, its translational velocity in a linear flow is non-zero. In contrast, the expression for relative angular velocity (2.5) contains an even combination of d_i, and is thus unaffected by the transformation $d_i \to -d_i$.

While the above arguments provide direct expressions for the translational and rotational velocities of the particle, one has to solve the Stokes equations to determine the scalar coefficients B, f_1 and f_2. As mentioned above, for arbitrary β this a difficult task; therefore, to make progress we invoke the limit $\beta \ll 1$ in which the slip length is much smaller than the particle radius. To proceed, the velocity and pressure fields are written as regular perturbation expansions in β, viz

$$u_i = u_i^{(0)} + \beta u_i^{(1)} + O(\beta^2), \quad p = p^{(0)} + \beta p^{(1)} + O(\beta^2), \tag{2.9}$$

where the zeroth-order fields $u_i^{(0)}$ and $p^{(0)}$ correspond to a no-slip particle translating with velocity U_i and rotating with angular velocity $\omega_i - \omega_i^{\infty}$ relative to the linear flow. The first-order velocity $u_i^{(1)}$ and pressure $p^{(1)}$ satisfy the Stokes equations and vanish at infinity. Most importantly, the first-order slip flow $u_i^{(1)}$ at $r = a$ is forced by the normal component of the zeroth-order rate of strain $E^{(0)}_{ij} n_j$. The first-order fields are computed using Lamb's solution for Stokes flow; full details of the calculations are given in appendix A. In fact, using the approach described in appendix A, one can calculate the complete grand resistance matrix (Kim & Karrila 2005) for the slip–stick particle, and this is presented in appendix B. The translational velocity U_i and relative angular velocity $\omega_i - \omega_i^{\infty}$ are determined by asserting that the total force $F_i = F_i^{(0)} + \beta F_i^{(1)}$ and total torque $T_i = T_i^{(0)} + \beta T_i^{(1)}$ on the particle are equal to zero. The scalar constants calculated in appendix A to leading order in β are summarized in table 1. With this information, we can compute the dynamics of the centre of mass

Scalar	Functional form
B	$-(15/16)\sin^2\alpha\cos\alpha$
f_1	$-(5/8)\sin^2\alpha\left(1+\cos^2\alpha\right)$
f_2	$(5/16)\sin^2\alpha\left(-5\sin^2\alpha+4\right)$
g_1	$-(15/8)(1-\cos\alpha)^2\left(\cos^3\alpha+2\cos^2\alpha+3\cos\alpha+4\right)$
g_2	$(75/16)\cos\alpha\sin^2\alpha\left(7\cos^2\alpha-3\right)$
g_3	$-(75/8)\cos^3\alpha\sin^2\alpha$

TABLE 1. The leading-order term in β for the various scalar constants appearing in the expressions for rotational velocity (2.5), translational velocity (2.6) and stress tensor (4.3).

and the orientation of a slip–stick sphere when placed in a general linear flow, and this is discussed in the following section.

3. Particle motion in a linear flow

In the previous section, we observed that the imposition of the force- and torque-free restrictions on the slip–stick sphere endows it with translational and rotational velocities that are, in most cases, non-zero. In this section, we explore the rich dynamics exhibited by a hydrodynamically Janus particle in a general linear flow, and in particular, a simple shear flow.

Consider a slip–stick sphere placed in the general linear flow $u_i^\infty = E_{ij}^\infty x_j + (1/2)\epsilon_{ijk}\omega_j^\infty x_k$. The governing equations for the motions of the director and the centre of mass x_i^P of the slip–stick sphere are as follows:

$$\left.\begin{aligned}\frac{\mathrm{d}d_i}{\mathrm{d}t} &= \epsilon_{ijk}\omega_j d_k = \epsilon_{ijk}\omega_j^\infty d_k + \beta B\left(E_{ij}^\infty d_j - d_i E_{jk}^\infty d_j d_k\right),\\ \frac{\mathrm{d}x_i^P}{\mathrm{d}t} &= \left(E_{ij}x_j + \frac{1}{2}\epsilon_{ijk}\omega_j^\infty x_k\right)x_j^P + a\beta\left(f_1 E_{ij}^\infty d_j + f_2 d_i d_j d_k E_{jk}^\infty\right).\end{aligned}\right\} \tag{3.1}$$

Note that the evolution equation of the director is identical to that of an axisymmetric particle (e.g. see Kim & Karrila 2005). Therefore, the director is expected to describe Jeffery orbits in a simple shear flow analogous to a spheroid. The Bretherton constant for the slip–stick sphere is βB. As noted by Dorrepaal (1978), the sign of the Bretherton constant is indicative of the geometry of an object; for example, prolate (oblate) spheroids have positive (negative) values of the Bretherton constant. In the case of a spherical cap, the Bretherton constant is negative, indicating the oblate character of the cap's shape (Dorrepaal 1978). In contrast, the asymmetric doublet of Nir & Acrivos (1973) is a prolate body with positive Bretherton constant. Interestingly, for the slip–stick sphere, the sign of the Bretheron constant βB depends on the value of the slipping angle α. For $0 \leqslant \alpha < \pi/2$, $\beta B < 0$, so that the slip–stick sphere is oblate, whereas for $\pi/2 < \alpha \leqslant \pi$, $\beta B > 0$, hence the slip–stick sphere is prolate.

The hydrodynamic aspect ratio $\mathscr{R}$ of the equivalent spheroid is

$$\mathscr{R} = \sqrt{\frac{1+\beta B}{1-\beta B}} \approx \sqrt{\frac{1-(15/16)\beta\sin^2\alpha\cos\alpha}{1+(15/16)\beta\sin^2\alpha\cos\alpha}} \approx 1 - \frac{15}{16}\beta\sin^2\alpha\cos\alpha + O(\beta^2). \tag{3.2}$$

Notably, when the slipping angle α is equal to 0, π or $\pi/2$, the aspect ratio $\mathscr{R}$ is equal to unity. The dynamics of the director for these cases will be identical to that of an

isotropic sphere – a rotation with the ambient angular velocity ω_i^∞. These behaviours will be explained physically in subsequent paragraphs of this section.

Let us study the dynamics of the slip–stick sphere for the simple shear flow $u_3^\infty = \dot{\gamma} x_1$. For this flow, it is convenient to write the director in spherical coordinates as

$$\left.\begin{aligned} d_1 &= \sin\theta \sin\phi, \\ d_2 &= \cos\theta, \\ d_3 &= \sin\theta \cos\phi, \end{aligned}\right\} \tag{3.3}$$

where θ and ϕ are polar and equatorial angles, respectively. The governing equations simplify to

$$\left.\begin{aligned} \frac{\mathrm{d}\theta}{\mathrm{d}t} &= \frac{B}{4}\dot{\gamma} \sin 2\theta \sin 2\phi, \\ \frac{\mathrm{d}\phi}{\mathrm{d}t} &= -\frac{\dot{\gamma}}{2} + \beta\frac{B}{2}\dot{\gamma} \cos 2\phi, \\ \frac{\mathrm{d}x_i^P}{\mathrm{d}t} &= \dot{\gamma} x_1^P \delta_{i3} + a\beta\dot{\gamma}\left[\frac{f_1}{2}\left(\delta_{i1}d_3 + \delta_{i3}d_1\right) + f_2 d_i d_1 d_3\right]. \end{aligned}\right\} \tag{3.4}$$

To better understand the individual contributions of the rotational and straining components of the simple shear flow to the particle dynamics, we will split our discussion into three cases: (*a*) the sphere placed in an ambient rotating flow, (*b*) the sphere placed in a pure straining flow and (*c*) the sphere placed in the complete simple shear flow.

3.1. *Slip–stick sphere in the ambient rotating flow* $u_i^\infty = (\dot{\gamma}/2)(\delta_{i3}x_1 - \delta_{i1}x_3)$

In this rather trivial case, the governing equations for the translational velocity and the director reduce to

$$\left.\begin{aligned} \frac{\mathrm{d}\theta}{\mathrm{d}t} &= 0, \\ \frac{\mathrm{d}\phi}{\mathrm{d}t} &= -\frac{\dot{\gamma}}{2}, \\ \frac{\mathrm{d}x_i^P}{\mathrm{d}t} &= \frac{1}{2}\epsilon_{ijk}\omega_j^\infty x_k^P = \frac{\dot{\gamma}}{2}\left(\delta_{i3}x_1^P - \delta_{i1}x_3^P\right). \end{aligned}\right\} \tag{3.5}$$

The slip–stick sphere thus executes a rotational motion with an angular velocity identical to that of the ambient field, and simply translates with the local ambient velocity evaluated at the centre of the sphere.

3.2. *Slip–stick sphere in the pure straining flow* $u_i^\infty = (1/2)\dot{\gamma}(\delta_{i3}x_1 + \delta_{i1}x_3)$

For pure straining flow, governing equations (3.4) become

$$\frac{\mathrm{d}\theta}{\mathrm{d}t} = \beta\frac{B}{4}\dot{\gamma} \sin 2\theta \sin 2\phi, \tag{3.6a}$$

$$\frac{\mathrm{d}\phi}{\mathrm{d}t} = \beta\frac{B}{2}\dot{\gamma} \cos 2\phi, \tag{3.6b}$$

$$\frac{\mathrm{d}x_i^P}{\mathrm{d}t} = \frac{\dot{\gamma}}{2}\left(\delta_{i1}x_3^P + \delta_{i3}x_1^P\right) + a\beta\dot{\gamma}\left[\frac{f_1}{2}\left(\delta_{i1}d_3 + \delta_{i3}d_1\right) + f_2 d_i d_1 d_3\right]. \tag{3.6c}$$

Let us first examine the rotational behaviour of the sphere. Clearly, the dynamics of the equatorial angle ϕ is independent of the polar angle θ and thus may be examined separately. There are four steady states of the equatorial

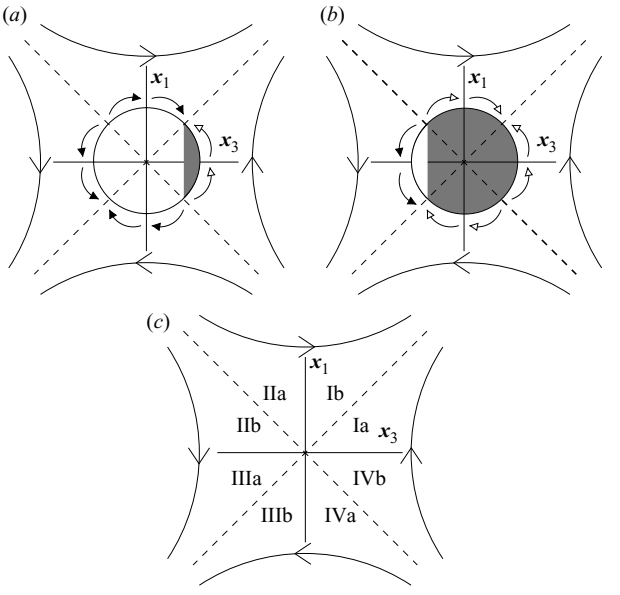

FIGURE 2. Why the quarter-slipping and three-quarter-slipping spheres rotate in opposite directions in pure straining flow. The shaded areas of the spheres in (*a*) and (*b*) represent their slipping portions. (*c*) The labelling convention employed in the text for the various octants Ia through IVb of the flow. The curved arrows with triangular heads near the sphere surface convey qualitatively the local torque acting on the surface due to the imposed flow. The arrows with filled triangular heads (in the no-slip regions) indicate a stronger torque than those with hollow triangular heads (in the slipping regions). 'Summing up the curved arrows' around the sphere yields the net torque. One can see that the total torque acting on the quarter sphere in (*a*) is negative which will result in a clockwise motion of the sphere. On the other hand, the three-quarter sphere in (*b*) will experience a positive torque of equal magnitude as the sphere in (*a*), and, in response, will rotate in the anticlockwise direction.

angle $\phi = (\pi/4, 5\pi/4), (3\pi/4, 7\pi/4)$. The brackets group together physically identical orientations of the sphere. Out of these, one pair represents a stable fixed point, while the other pair is unstable. The stability depends on the sign of the Bretherton constant B, which, in turn, depends on the degree of slipping of the sphere α. Before we examine the stability mathematically, it is instructive to consider the stability behaviour through physical arguments.

Let us first attempt to predict the direction of rotation of the sphere as a function of its orientation for the case of $\theta = \pi/2$ when the director is oriented in the plane of shear. It will be shown later that this is a stable steady state for the polar angle. Thus, if the sphere starts out with its director in the plane of shear, it will remain in the plane of shear. Consider a slip–stick sphere with a slipping angle $\alpha = \pi/4$ oriented along the x_3 axis (see figure 2*a*). We divide the flow field into eight octants (Ia, Ib, IIa, IIb, ..., IVb) as shown in figure 2(*c*), for purposes of this discussion. In figure 2(*a*), with $\alpha = \pi/4$ and $\phi = 0$, the negative torque on the sphere in octants Ib and IIa (no-slip) cancels the positive torque in octants IIb and IIIa (no-slip). The residual torque on the sphere arises from a balance between the negative torque in the no-slip octants IIIb and IVa, and weak positive torque in the slip octants IVb and Ia, which results in a net negative torque on the sphere. Hence, as the sphere is torque free, it rotates in a clockwise direction. Thus, for $\alpha = \pi/4$ and $\phi = 0$, ω_2 should be negative.

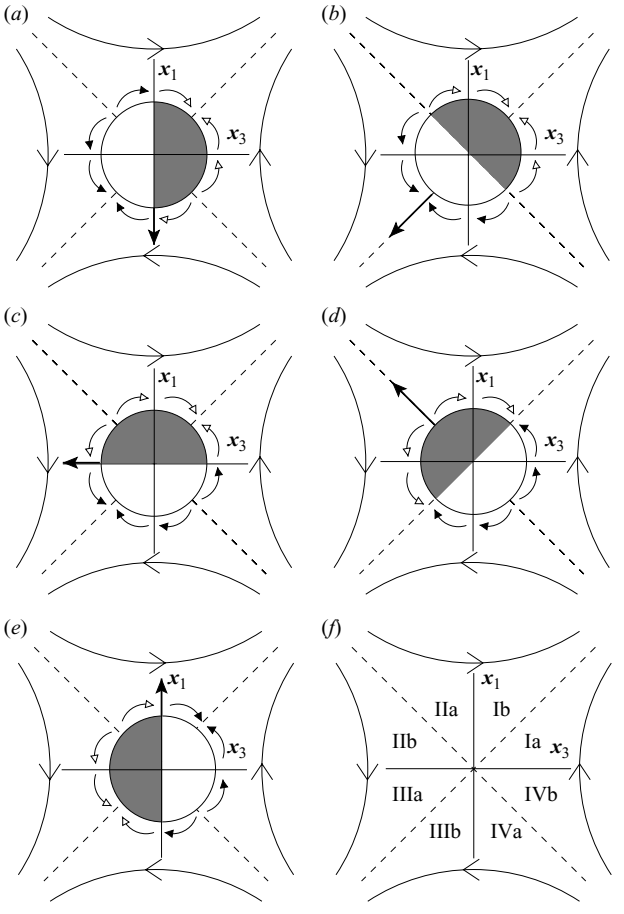

FIGURE 3. Why the half-slipping sphere does not rotate in pure straining flow. The legend is the same as in figure 2. Summing up the arrows over each sphere, one can see that the solid arrows in the no-slip regions always cancel each other out, and the same is true for the hollow arrows in the slipping regions. Therefore, the net torque on the half-sphere is zero regardless of the orientation. The straight arrow with the dark triangular head in (*a*)–(*e*) shows the direction of the net force acting on the particle due to the flow. (*a*) $\phi = 0$; because of the symmetry of the half-sphere, there is a net force acting in both slip and no-slip portions only along the x_1 axis. However, the magnitude of the downward force over the no-slip region is greater than the upward force in the slip region, resulting in a net downward force. (*b*) $\phi = \pi/4$; there is an overall pulling force acting along the extensional axis in both the slipping and non-slipping regions. But since the pull in the no-slip region is stronger, the sphere is dragged along the extensional axis towards its no-slip face along $-d_i$. Similar explanations may be offered for (*c*)–(*e*).

Now consider a three-quarter-slipping sphere ($\alpha = 3\pi/4$) with $\phi = 0$ as shown in figure 2(*b*). In this case, the torques in octants IIa & Ib and Ia & IVb cancel out each other. A net positive torque acts on the particle due to the stronger positive torque on the no-slip octants IIb and IIIa than the weaker negative torque on the slip octants IIIb and IVa. Thus, for $\alpha = 3\pi/4$ with $\phi = 0$, ω_2 should be positive. This reversal of the direction of the angular velocity with the transformation $\alpha \rightarrow \pi - \alpha$ may be demonstrated with such physical arguments for arbitrary α and orientation ϕ. This is supported by the factor $\cos\alpha$ in the expression for B (see table 1). Note that when $\alpha = \pi/2$, the angular velocity is identically zero. This may be explained

with the diagrams in figure 3. From these figures, it is seen that for any orientation of the half-slipping sphere, there are always two no-slip and two slip octants with positive torque, and two no-slip octants and two slip octants with negative torque. The net torques in the slip and no-slip halves of the sphere are exactly zero, resulting in a torque-free particle.

Consider again the quarter-slipping sphere as shown in figure 4 in various orientations. figure 4(*b*) shows the slip–stick sphere oriented in the steady-state configuration of $\phi = 7\pi/4$. In this position, the torques in the no-slip octants Ia through IIIB cancel each other exactly, so also do the torques in the slip octants IVa and IVb. Thus, the net torque on the sphere in this position is identically zero. In fact, this argument for zero angular velocity of the sphere is valid irrespective of the value of α. Similar arguments may be used to demonstrate that $\phi = \pi/4, 3\pi/4$ and $7\pi/4$ are also steady-state orientations. To determine the stability of these orientations, we study the effect of imposing a perturbation in ϕ from these steady states. The steady state is stable if the perturbation decays in time, and is unstable if it does not. For purposes of simplicity, let us take this perturbation to be $\pm\pi/4$. Using the arguments presented in the previous paragraph, one can see that starting from either of the positions $0, \pi/2, \pi$ or $3\pi/2$ (left panel in figure 4), the sphere will eventually orient itself along the compressional axis ($\phi = 3\pi/4$ or $\phi = 7\pi/4$) (right panel in figure 4). Thus, for a quarter-slipping sphere, the orientations along the compressional axis are stable, while orientations along the extensional axis ($\phi = \pi/4, 5\pi/4$) are unstable. This result applies for all angles $\alpha < \pi/2$. In a similar fashion, it may be demonstrated (see figure 5) that a three-quarter-slipping sphere always tends to orient itself along the extensional axis of the straining flow.

The above predictions may be corroborated by performing a linear stability analysis of governing equations (3.6*a*) and (3.6*b*). It may be shown that one eigenvalue for this equation is $e_1 = -\beta B \sin 2\phi^*$, where ϕ^* is a steady-state solution to (3.6*b*). Thus, for the combinations $\phi^* = \pi/4$ or $5\pi/4$ and $B < 0$ ($0 < \alpha < \pi/2$), and $\phi^* = 3\pi/4$ or $7\pi/4$ and $B > 0$ ($\pi/2 < \alpha < \pi$), this eigenvalue is negative, implying that the steady states are stable. This is exactly what is predicted by the physical arguments presented above. The second eigenvalue e_2 is simply $-e_1 \cos(2\theta^*)/2$. The steady-state values for θ from (3.6*a*) are $\theta^* = 0, \pi/2, \pi$. It may be seen that provided e_1 is negative, e_2 is negative only for $\theta^* = \pi/2$. Therefore, the sphere always ultimately orients itself into the plane of the pure straining flow. It is important to note that the dynamics of the director is only a function of θ and ϕ and is, therefore, independent of the position of the particle in the flow. Thus, given an initial orientation, the evolution of the director will be the same irrespective of its initial position.

Now consider the translational motion of the sphere as described by (3.6*c*). Let us begin with the sphere placed at the origin of the flow. In this position, the translational velocity is $O(a\beta\dot{\gamma})$ and depends strongly on its orientation. If the director is initially along the x_3 axis, then for any value of α, the particle is displaced in the negative x_1 direction. This may be understood by examining, for instance, figure 3(*a*) showing the quarter-slipping sphere. The forces acting on the sphere in octants Ib & IIa and IIIb & IVa balance each other exactly. The forces that act in the no-slip octants IIb and IIIa and the slip octants IVb and Ia when integrated act only in the negative and positive x_1 directions, respectively. Since the no-slip force is greater than the slip force, the net force acting on the particle is in the negative x_1 direction. The sphere, therefore, moves along the negative x_1 axis to balance this force. These arguments may be applied for arbitrary α to show that the sphere will move only in the negative x_1 direction when it is placed at the flow origin with $d_i = \delta_{i3}$. Similarly, when $d_i = -\delta_{i3}$, the sphere is displaced in the positive x_1 direction.

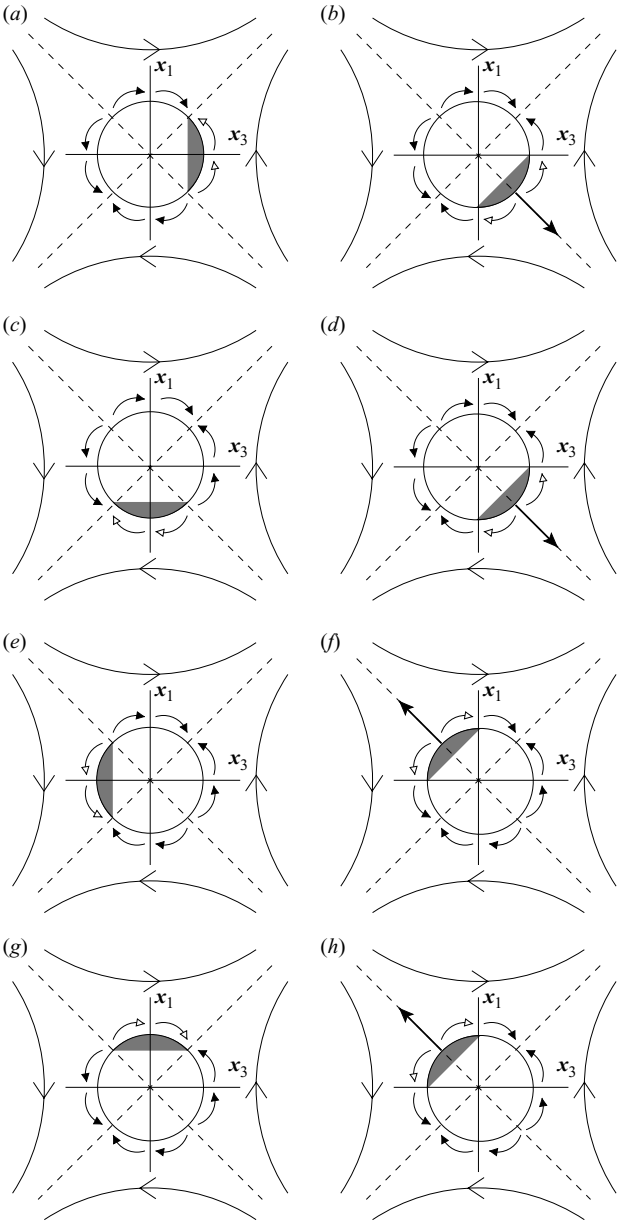

FIGURE 4. The stable orientational configurations of a quarter sphere in a pure straining flow. For the meanings of the arrows, refer to the caption of figure 2. The left panel shows different initial orientations of the sphere, while the right panel displays the final orientations that these initial configurations evolve into. One can see by summing up the arrows that the net torques for all the orientations in the right panel are zero. In (a) with $\phi = 0$, summing up the arrows in the initial configuration indicates that the sphere should experience a negative torque, and consequently it settles into the steady state along the compressional axis with $\phi = 7\pi/4$ as shown in the right panel (b). On the other hand, when ϕ is initially equal to $3\pi/2$ (c, d), the sphere experiences a positive torque and again returns to the steady configuration shown in the right panel. Similarly, when starting with $\phi = \pi$ and $\phi = \pi/2$, the sphere again rotates to settle along the compressional axis, but this time with $\phi = 3\pi/4$.

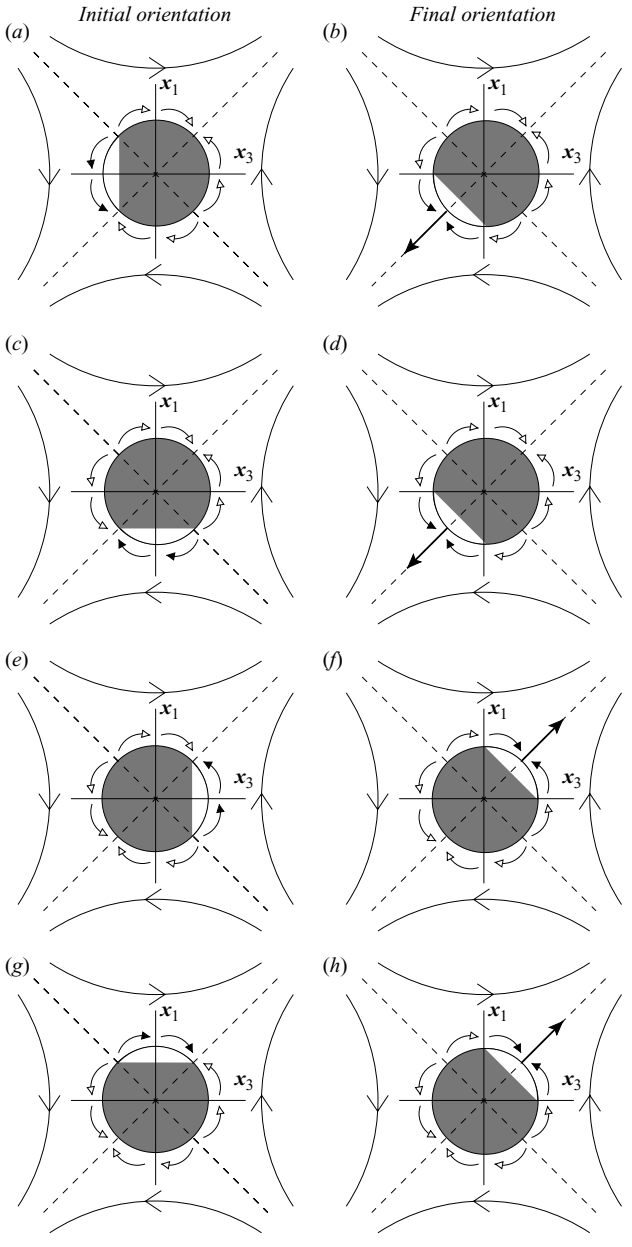

FIGURE 5. The stable orientational configurations of a three-quarter sphere in a pure straining flow. For the meanings of the arrows, refer to the caption of figure 2. Using arguments identical to those put forth in the caption for figure 4, one can see that the sphere always rotates to arrange itself along the orientationally closer extensional axis ($\phi = \pi/4$ or $\phi = 5\pi/4$).

Consider the case when the sphere is oriented along the extensional axis of the flow. There is a net force acting on the sphere along the extensional axis towards the no-slip side (along $-d_i$), irrespective of α. On the other hand, when the sphere is oriented with its director along the compressional axis, a net force acts along the compressional axis towards the slip side (along d_i). These trends may be easily verified from (3.6c) and the expressions for the functions f_1 and f_2 in table 1. Once

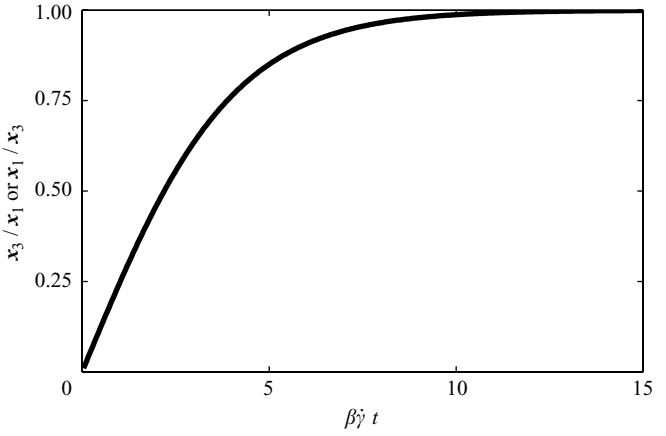

FIGURE 6. Plot of the evolution of the ratio of the in-plane coordinates x_3/x_1 (for $\phi_0 = 0, \pi$) or x_1/x_3 (for $\phi_0 = \pi/2, -\pi/2$) for $\beta = 0.1$. The results are identical for $\alpha = \pi/4$ and $\alpha = 3\pi/4$.

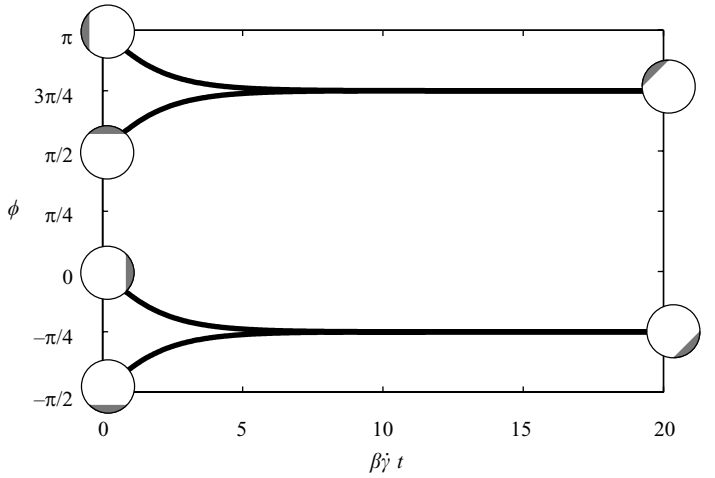

FIGURE 7. Plot of the evolution of the orientation of the director ϕ for $\beta = 0.1$ and $\alpha = \pi/4$.

the sphere is displaced from the centre of the straining flow, its translational motion is dominated by the component arising from the ambient straining flow [the first term in (3.6*c*)] which is independent of the orientation of the sphere. Said differently, the centre-of-mass motion becomes independent of the director dynamics once the sphere is sufficiently far away from the centre of the flow.

In figures 6 and 7, we have shown the dynamics of a quarter-slipping sphere for different initial orientations. From the figures, it may be seen that irrespective of the initial orientation ϕ_0, the particle finally aligns itself with the compressional axis of the flow in the plane of shear, while the centre of mass moves close to extensional axis once the particle leaves the flow centre. For a three-quarter-slipping sphere, the motion of the centre of mass eventually is, again, along the extensional axis away from the flow centre, but this time it orients with the extensional axis (see figure 8).

The particle also has four steady-state positions corresponding to specific initial orientations, two each on the compressional and extensional axes, which are symmetrically placed around the flow origin at a distance of $O(\beta a)$. For example,

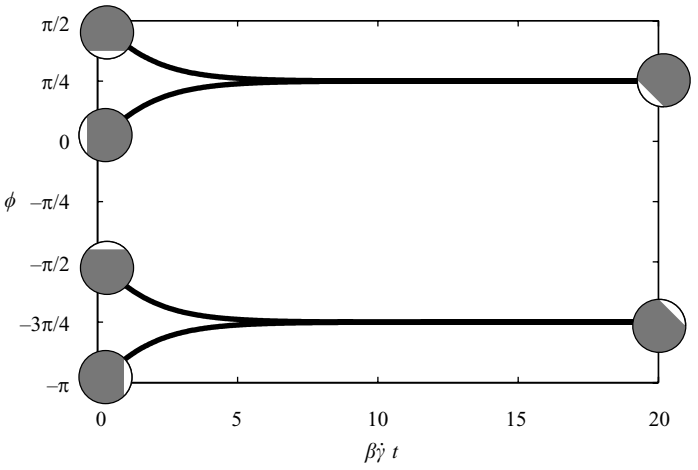

FIGURE 8. Plot of the evolution of the orientation of the director ϕ for $\beta = 0.1$ and $\alpha = 3\pi/4$.

if the particle is on the compressional axis (quadrant II) with $\phi_0 = 3\pi/4$, the steady position is achieved by a balance between the straining flow sweeping the particle towards the origin and the outward translational motion due to the response of the particle to the external flow. These steady-state positions are, however, unstable.

3.3. *Slip–stick sphere in the simple shear flow* $u_3^\infty = \dot{\gamma} x_1$

To understand the motion of the hydrodynamically Janus sphere in the simple shear flow $u_3^\infty = \dot{\gamma} x_1$, we simply combine the results of the purely rotational and straining cases. The governing equations have already been presented in (3.4), and although it is possible to obtain an analytical solution to these equations (for the actual formulas, see Nir & Acrivos 1973), we employ a numerical method here. The numerically evaluated results of the centre of mass and particle trajectories are shown in figures 9–12. The rotational motion is the sum of rigid body motion about the x_2 axis and a rotation due to the inability of the sphere to deform in the straining flow, which results in Jeffrey orbits as alluded to earlier in this section. However, since the contribution of the straining flow to the rotation is $O(\beta)$, the orbits are only weakly perturbed from perfect circles (see figure 12*b*).

The motion of the centre of mass of the sphere is much more interesting. The particle may either execute a periodic motion, or experience a constant displacement along the x_3 (flow) axis at the end of every period of rotation. The type of trajectory depends on whether the director is parallel to the flow as the sphere passes through the zero velocity plane. If this is the case (i.e. $\phi = 0$ when $x_1 = x_3 = 0$), then the trajectory is a closed orbit (see figures 9 and 12) whose size scales as $a\beta$. If this condition is not satisfied, then the sphere experiences a net drift along the x_3 axis after each period of rotation (see figures 10 and 11). This may also be demonstrated by examining the analytical solutions to the governing equations, but in the interest of brevity, we shall not pursue this here.

The trajectories in figures 10 and 11 may be understood with the aid of our discussion of the translational motion of the Janus sphere in pure straining flow. For example, consider the drift of the half-slipping sphere initially placed at the flow origin with orientation $\phi_0 = \pi/2$, as shown in figure 11(*c*). From figure 3(*c*), the sphere experiences an instantaneous drift along the $-x_3$ direction. At the same time, it rotates with the ambient flow in the clockwise direction, resulting in an equatorial

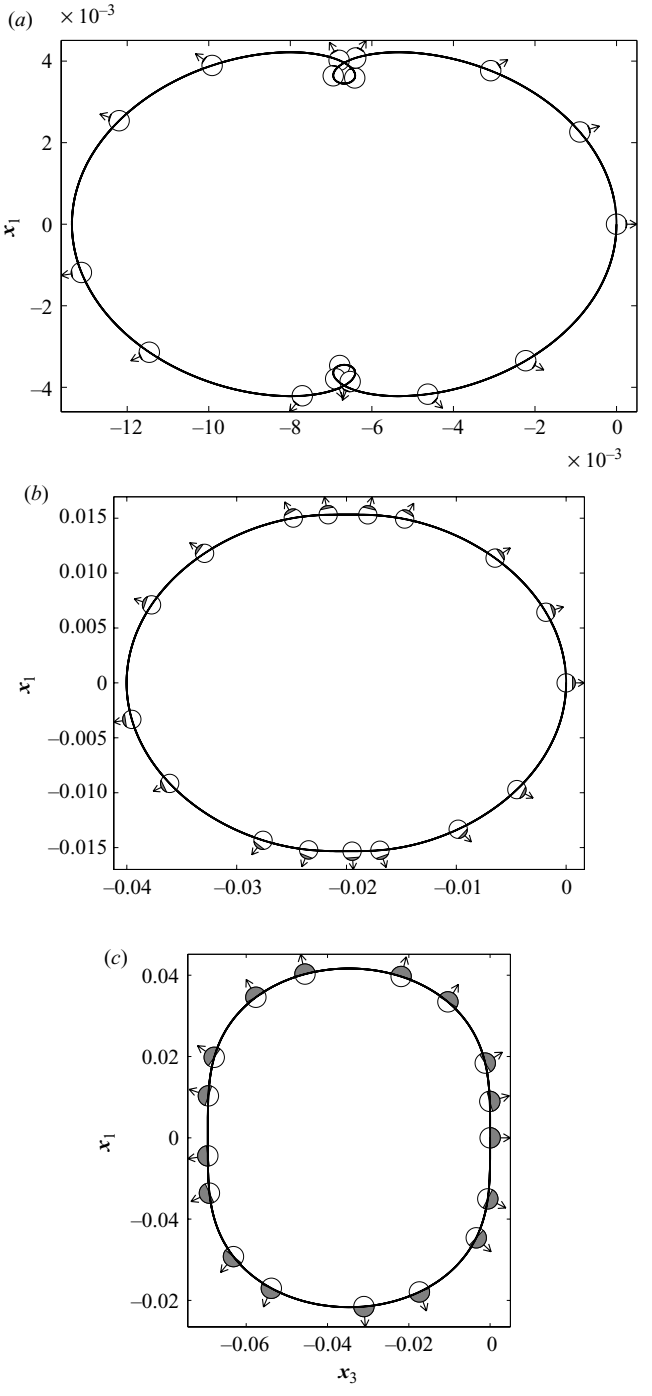

FIGURE 9. Closed-orbit trajectories (solid lines) with sphere orientation (arrows) for $\beta = 0.05$ and different α. The initial position for all these simulations is the origin. The sphere starts out and remains in the plane of shear ($\theta = \pi/2$), and the initial orientation ϕ_0 is zero. The parameter α for (*a*), (*b*) and (*c*) are $\pi/8$, $\pi/4$ and $\pi/2$, respectively.

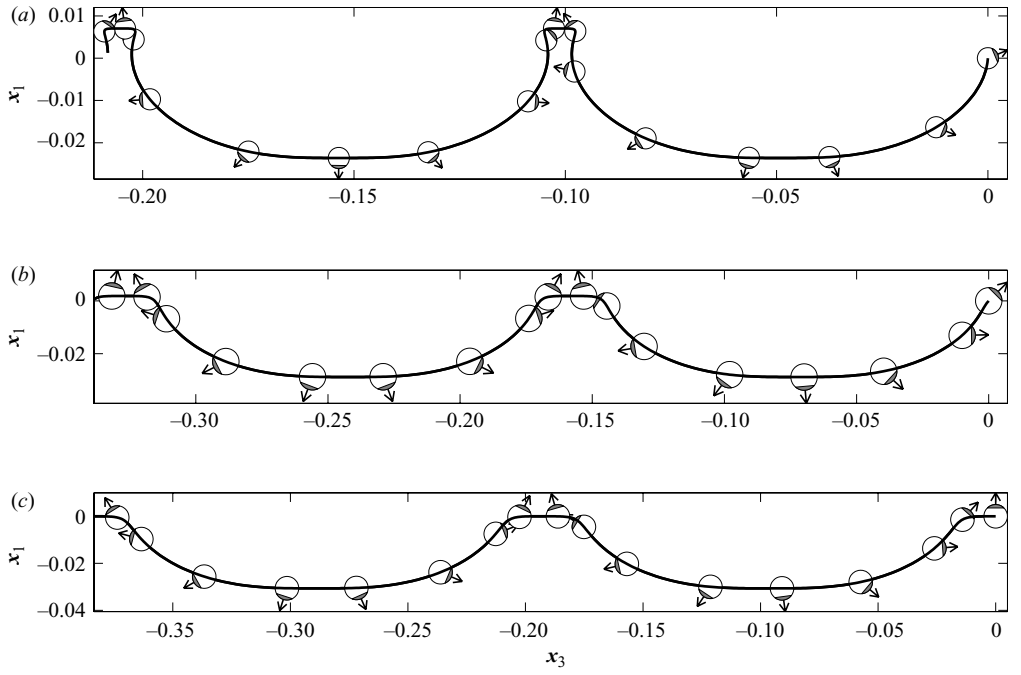

FIGURE 10. Non-periodic trajectories (solid lines) with sphere orientation (arrows) for different ϕ_0 with $\alpha = \pi/4$ and $\beta = 0.05$. The integration with time was carried out up to $\dot{\gamma}t = 25$. The initial position for all these simulations is the origin. The sphere starts out and remains in the plane of shear ($\theta = \pi/2$). The initial orientations ϕ_0 for (*a*), (*b*) and (*c*) are $\pi/8$, $\pi/4$ and $\pi/2$, respectively.

angle $\phi < \pi/2$. For this orientation, the translational velocity of the sphere acquires a component in the $-x_1$ direction (e.g. see figure 3*b*) and the sphere drifts below the zero velocity streamline. Subsequently, it is swept by the shear flow further in the $-x_3$ direction (which also explains the fact that the direction of the net drift in figures 10 and 11 is always along the negative x_3 direction). But the x_1 component of the sphere velocity is still determined only by its orientation in the local pure straining flow. Therefore, as the sphere rotation crosses $\phi = -\pi/2$ (the minimum in the trajectory in figure 11*c*), its velocity in the x_1 direction switches from being negative to positive. Eventually, it reaches the zero velocity streamline and the cycle starts again *ad infinitum*.

The results here are qualitatively similar to the trajectories of an asymmetric doublet (Nir & Acrivos 1973) and spherical cap (Dorrepaal 1978) in a simple shear flow. In particular, analogous to the slip–stick sphere, both the asymmetric doublet and spherical cap execute periodic trajectories only if they are oriented along the flow when their centre of rotation is in the zero velocity plane. Otherwise, the doublet and cap experience a net displacement in the flow direction. Note that while the slip–stick sphere, asymmetric doublet and spherical cap may migrate along the flow direction, these do not experience a net translation transverse to the flow. More generally, in fact, as shown by Bretherton (1962), any body of revolution that undergoes a periodic rotational motion in a simple shear flow will not execute a net migration across streamlines.

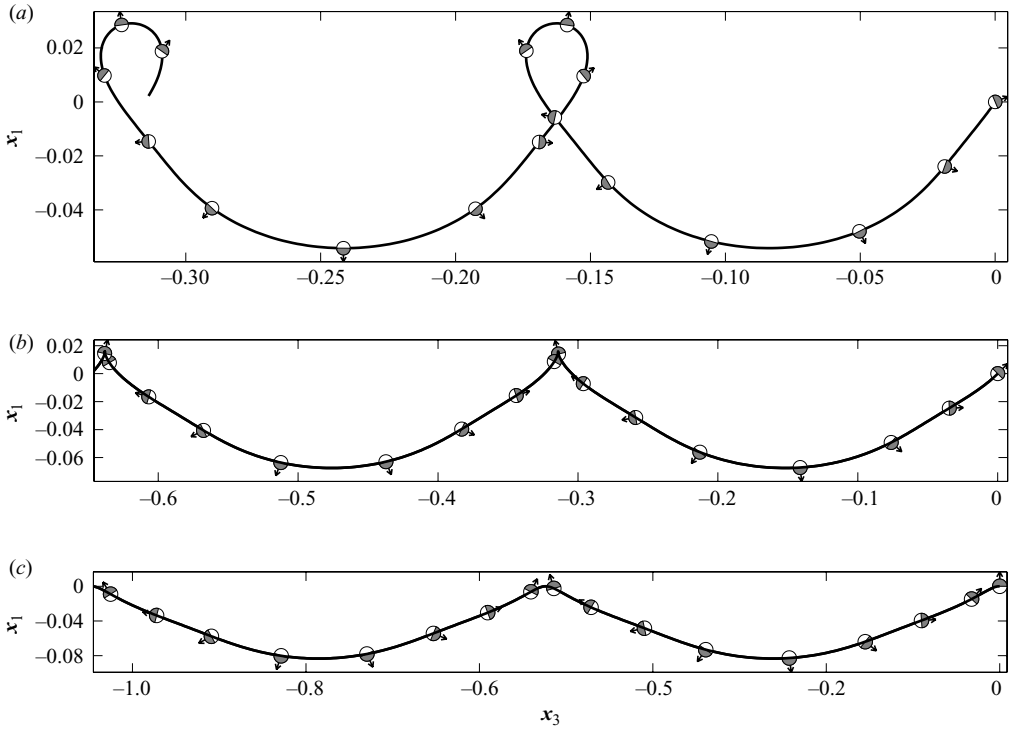

FIGURE 11. Non-periodic trajectories (solid lines) with sphere orientation (arrows) for different ϕ_0 with $\alpha = \pi/2$ and $\beta = 0.05$. The integration with time was carried out up to $\dot{\gamma}t = 25$. The initial position for all these simulations is the origin. The sphere starts out and remains in the plane of shear ($\theta = \pi/2$). The initial orientations ϕ_0 for (*a*), (*b*) and (*c*) are $\pi/8$, $\pi/4$ and $\pi/2$, respectively.

4. Rheological properties

In this section, we consider the rheology of a dilute suspension of Janus slip–stick spheres. In a linear flow, a slip–stick particle can translate and rotate such that there is no net force or torque on it; however, it cannot deform with the local straining motion of the fluid. This leads to an increase in the average, or macroscopic, stress of a suspension of such particles. As shown by Batchelor (1970), for a homogeneous suspension of N force- and torque-free particles, the average stress $\langle \Sigma_{ij} \rangle$ is given by

$$\langle \Sigma_{ij} \rangle = -\langle p \rangle_f \delta_{ij} + 2\mu_0 \langle E_{ij} \rangle + n \langle S_{ij} \rangle, \tag{4.1}$$

where $\langle \dots \rangle$ denotes an average over the entire suspension (particles plus suspending fluid) for a given instantaneous configuration, $\langle \dots \rangle_f$ denotes an average over the fluid phase only, $n = N/V$ is the number density of particles in a volume V, and the average particle stresslet $\langle S_{ij} \rangle$ is defined as a number average, $\langle S_{ij} \rangle = (1/N) \Sigma_{p=1}^{N} S_{ij}^p$. The contribution to the average stresslet from a single particle is

$$S_{ij}^p = \frac{1}{2} \oint [(x_i \sigma_{jk} n_k + x_j \sigma_{ik} n_k) - 2\mu_0 (u_i n_j + u_j n_i)] \mathrm{d}S; \tag{4.2}$$

the integral is over the surface of the particle, $S = S_1 \cup S_2$ as defined in figure 1. In the above, note that while the slip–stick particle is rigid, the tangential slip velocity

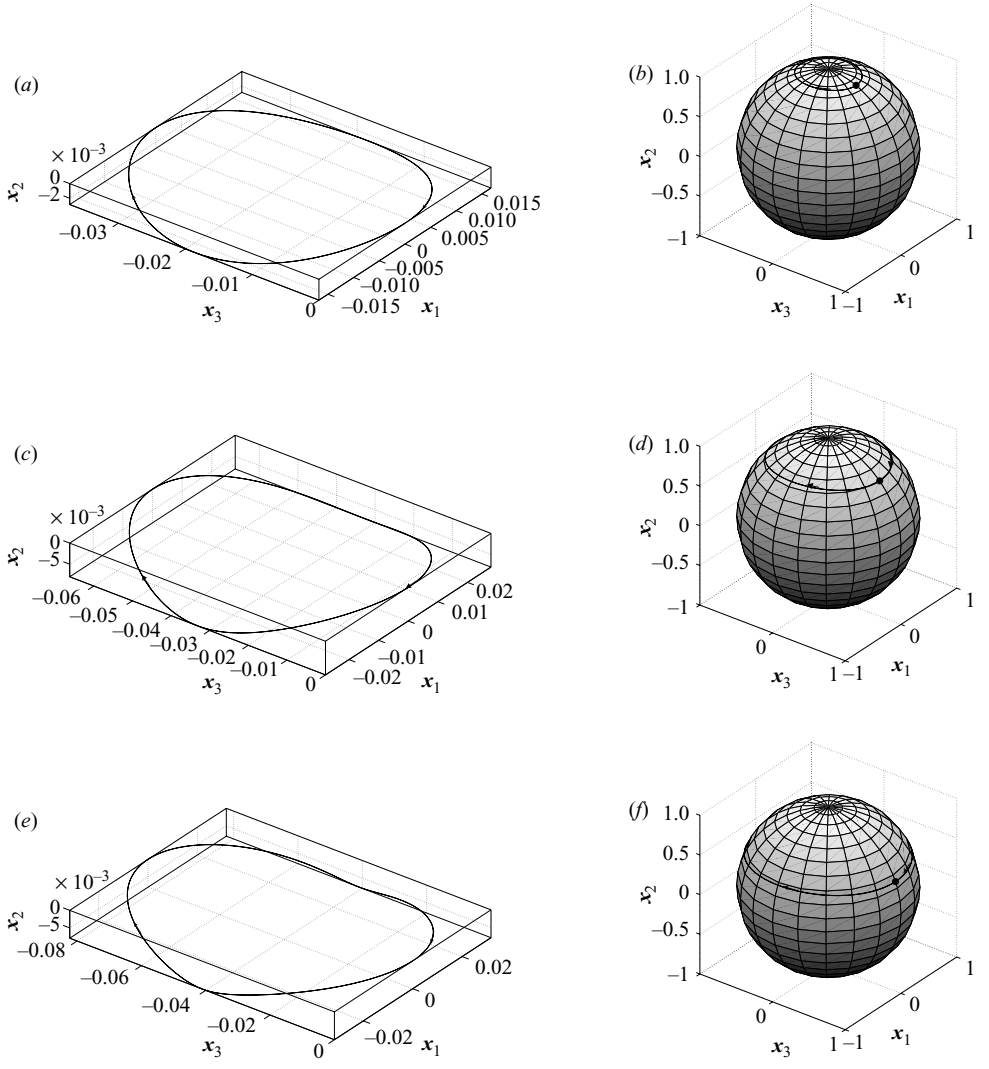

FIGURE 12. Three-dimensional periodic trajectories (solid lines) of the centre of mass (left panel) of the sphere and its director (right panel) for different initial values of θ with $\beta = 0.05$, $\alpha = \pi/4$ and an initial value of 0 for ϕ. The initial polar angle θ_0 of the director is $\pi/8$ for (a) and (b), $\pi/4$ for (c) and (d) and $3\pi/8$ for (e) and (f). In the right panel, the dot represents the initial orientation of the sphere. The arrows indicate the direction of motion and rotation in the left and right panels, respectively.

on the slipping portion $S_{p,1}$ does not vanish; hence, there is a contribution to the off-diagonal components of the particle stress from the velocity terms in the integral.

For a sufficiently dilute suspension, interactions between slip–stick spheres are negligible, and particle stress (4.2) can be computed from the solution of the Stokes equations for a single slip–stick sphere in a linear flow as described in appendix A. Moreover, if the initial orientations of each of the N particles are the same, they will contribute an equal amount to the average stresslet; thus $\langle S_{ij} \rangle = S^p_{ij}$.

From the linearity of the Stokes equations and because the orientation of a slip–stick particle is specified uniquely by d_i, the average stresslet can also be written in

the general form (Ericksen 1959)

$$\langle S_{ij}\rangle = \frac{20\pi}{3}\mu_0 a^3 E^{\infty}_{ij} + \frac{4\pi}{3}\mu_0 a^3\beta[g_0\delta_{ij}d_k d_l E^{\infty}_{kl} + g_1 E^{\infty}_{ij} + g_2 d_i d_j d_k d_l E^{\infty}_{kl} + g_3(d_i d_k E^{\infty}_{jk} + d_j d_k E^{\infty}_{ik})], \quad (4.3)$$

where the first term on the right-hand side of (4.3) is the stresslet for a no-slip sphere in a linear flow. In the small-slip-length limit ($\beta \ll 1$), the g_i scalars are dimensionless functions of the slip–stick dividing angle α only. A detailed discussion of the computations used to determine the g_i functions can be found in appendix A, and their functional forms are presented in table 1.

In appendix D, it is shown that in the dilute (single particle) limit, the trace of the stresslet must equal zero. Formally, from the above equation, the trace is given by

$$\langle S_{ii}\rangle = \frac{4\pi}{3}\mu_0 a^3\beta(3g_0 + g_2 + 2g_3)d_k d_l E^{\infty}_{kl}, \quad (4.4)$$

which implies that $3g_0 + g_2 + 2g_3 = 0$. Therefore, the stresslet may be re-written in the manifestly traceless form

$$\langle S_{ij}\rangle = \frac{20\pi}{3}\mu_0 a^3 E^{\infty}_{ij} + \frac{4\pi}{3}\mu_0 a^3\beta\left[g_1 E^{\infty}_{ij} + g_2(d_i d_j - \frac{1}{3}\delta_{ij})d_k d_l E^{\infty}_{kl} + g_3(d_i d_k E^{\infty}_{jk} + d_j d_k E^{\infty}_{ik} - \tfrac{2}{3}\delta_{ij}d_k d_l E^{\infty}_{kl})\right]. \quad (4.5)$$

It is instructive to consider the rheological response to the simple shear flow $u_3 = \dot\gamma x_1$. In this case, the $\boldsymbol{i_3}$, $\boldsymbol{i_1}$ and $\boldsymbol{i_2}$ unit vectors represent the flow, gradient and vorticity directions, respectively, and the first and second normal stress differences of the suspension are defined as $N_1 = \langle\Sigma_{33}\rangle - \langle\Sigma_{11}\rangle$ and $N_2 = \langle\Sigma_{11}\rangle - \langle\Sigma_{22}\rangle$, respectively. A straightforward calculation shows that

$$N_1 = \mu_0 c\dot\gamma\beta d_1 d_3(d_3^2 - d_1^2)g_2, \quad (4.6)$$

$$N_2 = \mu_0 c\dot\gamma\beta d_1 d_3((d_1^2 - d_2^2)g_2 + g_3), \quad (4.7)$$

where $c = 4\pi n a^3/3$ is the particle volume fraction. Substituting the components of the director d_i in spherical coordinates from (3.3) into the above equation, we find

$$\frac{N_1}{\mu_0 c\dot\gamma\beta} = \frac{1}{4}\sin^4\theta\sin 4\phi g_2, \quad (4.8)$$

$$\frac{N_2}{\mu_0 c\dot\gamma\beta} = \frac{1}{2}\sin^2\theta\sin 2\phi((\sin^2\theta\sin^2\phi - \cos^2\theta)g_2 + g_3). \quad (4.9)$$

Figure 13 plots g_2 and g_3 as a function of the slipping angle α. Of course, for an entirely no-slip or slipping sphere ($\alpha = 0$ or $\alpha = \pi$, respectively), g_2 and g_3 equal zero. In these trivial cases, the normal stress differences vanish as the particle surface is spherically symmetric. For a half-slipping sphere ($\alpha = \pi/2$), we see, again, that $g_2 = g_3 = 0$, which implies both normal stress differences are zero regardless of the orientation of the sphere. To offer a simple explanation for this somewhat surprising result, let us consider the case where the director lies in the plane of shear, $\theta = \pi/2$. In figure 14 we sketch the compressive and tensile (normal) stresses acting on a half-slipping sphere for various orientations of the director in the shear plane. For example, in figure 14(*b*) ($\phi = \pi/4$) the compressive stress acting over the no-slip surface in octants IIb and IVa is balanced by the tensile stress on the no-slip surface in the extensional quadrant III of the flow. Similarly, the compressive stress acting on the slipping surfaces in octants IIa and IVb is matched by the tensile stress in extensional

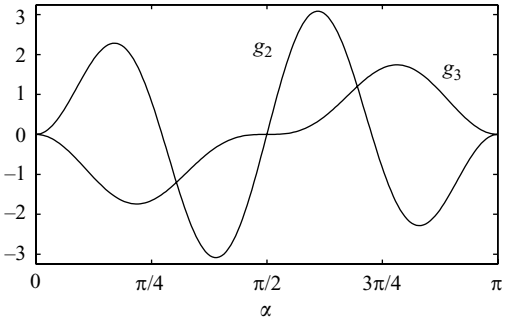

FIGURE 13. Plot of the stress functions g_2 and g_3 versus the slipping angle α.

quadrant I. Consequently, there is no net compressive or tensile stress on the particle and thus the normal stress differences N_1 and N_2 equal zero. Similar arguments may be applied to the four remaining subfigures in figure 14. The key point is that for a half-slipping sphere, there always exist two octants each of compressive no-slip stress, compressive slip stress, tensile no-slip stress and tensile slip stress.

We now consider the normal stress differences N_1 and N_2 for other slipping angles. Figure 15 plots the scaled second normal stress difference, $N_2/\mu_0 c\dot{\gamma}\beta$, as a function of the director orientation ϕ in the shear plane ($\theta = \pi/2$) for a quarter-slipping and three-quarter-slipping spheres, respectively. In both cases, N_2 vanishes when the director is parallel to the velocity or velocity-gradient axes. For a quarter-slipping sphere, as ϕ increases from zero, N_2 becomes increasingly negative, until $\phi \approx \pi/4$ at which point it reaches a minimum value. Beyond this N_2 increases (passing through zero at $\phi = \pi/2$) until a positive maximum is reached at $\phi \approx 3\pi/4$, after which N_2 decreases and becomes zero at $\phi = \pi$. Again, one may offer a simple explanation for this behaviour. In figure 16, we sketch the normal stresses acting on a quarter-slipping sphere for six orientations: $\phi = 0$, $\pi/4$, $\pi/2$, π, $3\pi/2$ and π. In each subfigure, there are six octants of no-slip stress and two octants of slip stress (lesser in magnitude). Following the arguments used for a half-slipping sphere, if the director is parallel to the velocity or velocity-gradient axis – figures 16(a), 16(c) and 16(e) – the compressive and tensile stresses balance such that there is zero net normal stress, and therefore no normal stress differences. However, if the director is aligned with the extensional axis of the flow $\phi = \pi/4$ (figure 16b) there is a net compressive stress acting on the sphere along the compressional axis of the flow. Since normal stresses are negative in compression by convention, this implies that $\langle \Sigma_{33} \rangle = \langle \Sigma_{11} \rangle < 0$ and thus $N_1 = \langle \Sigma_{33} \rangle - \langle \Sigma_{11} \rangle = 0$ and $N_2 = \langle \Sigma_{11} \rangle - \langle \Sigma_{22} \rangle < 0$. Similarly, for $\phi = 3\pi/4$ (figure 16d), a net tensile stress acts along the extensional axis of the flow, giving $\langle \Sigma_{33} \rangle = \langle \Sigma_{11} \rangle > 0$, and thus $N_1 = \langle \Sigma_{33} \rangle - \langle \Sigma_{11} \rangle = 0$ and $N_2 = \langle \Sigma_{11} \rangle - \langle \Sigma_{22} \rangle > 0$.

For a three-quarter-slipping sphere N_2 is of opposite sign for a given value of ϕ as compared to that for a quarter-slipping sphere. This may be explained by reference to figure 17 in which are sketched the stresses acting on a three-quarter-slipping sphere for $\phi = \pi/4$ (and also a quarter-slipping sphere for comparison). For $\alpha = 3\pi/4$ there are six octants of slip stress and two octants of no-slip stress. Summing the stresses in the eight octants, we see that there is a net tension on the sphere along the extensional axis of the flow, implying that $N_1 = \langle \Sigma_{33} \rangle - \langle \Sigma_{11} \rangle = 0$ and $N_2 = \langle \Sigma_{11} \rangle - \langle \Sigma_{22} \rangle > 0$. Thus, for $\phi = \pi/4$, N_2 is of opposite sign for three-quarter and one-quarter-slipping spheres.

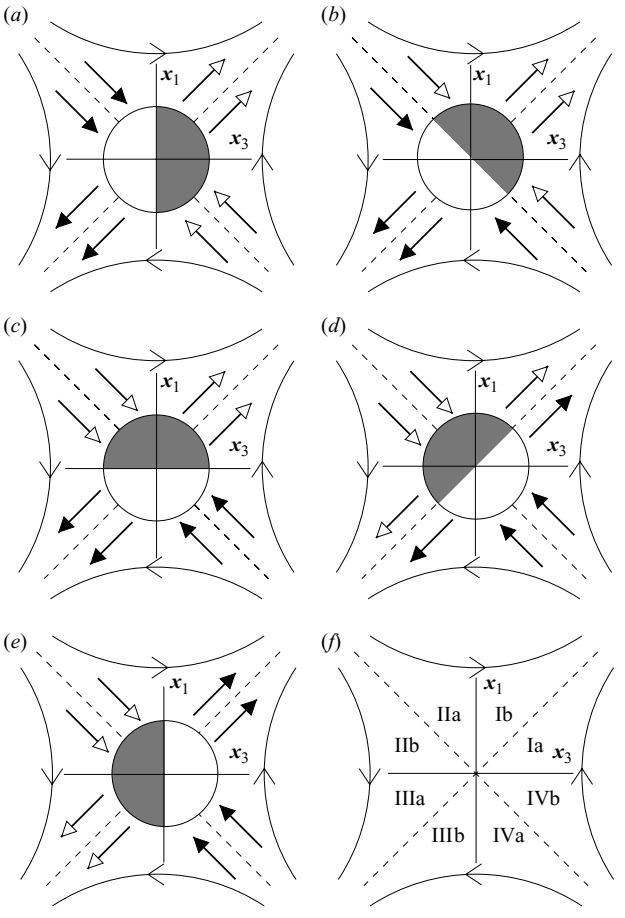

FIGURE 14. Why the normal stress differences N_1 and N_2 are zero for a half-slipping ($\alpha = \pi/2$) sphere. For each subfigure, the arrows represent qualitatively the normal stresses acting on the particle in the eight octants of the flow. An arrow pointing towards the particle indicates a compressive stress; conversely, an outward pointing arrow represents a tensile stress. Arrows with a filled arrowhead (acting on the no-slip portions of the sphere) signify a greater in magnitude stress than arrows with a hollow arrowhead (which act over the slipping portions). For each subfigure we see that there are always two octants of compressive stress acting on the no-slip portion of the sphere; however, these are balanced by the tensile stress exerted over two no-slip octants. A similar balance is realized over the slipping portions of the sphere. Thus, in each configuration there is no net normal stress on the particle and consequently the normal stress differences must vanish.

In the above discussion, we concluded that for a quarter or three-quarter-slipping sphere, the first normal stress difference N_1 is zero when the director is along the velocity or velocity-gradient axis. Furthermore, N_1 is zero if the director is aligned with the compressional or extensional axis of the shear flow, since, in these cases, the net compression or tension on the particle acts equally in the velocity and velocity-gradient directions. For intermediate values of ϕ, however, there is an imbalance in the normal stresses acting in the x_1 and x_3 directions that will lead to a non-zero N_1. This is clearly seen in figure 18 in which the scaled first normal stress difference, $N_1/\mu_0 c\dot{\gamma}\beta$, is plotted as a function of ϕ for $\alpha = \pi/4$ and $\alpha = 3\pi/4$. By analogy with

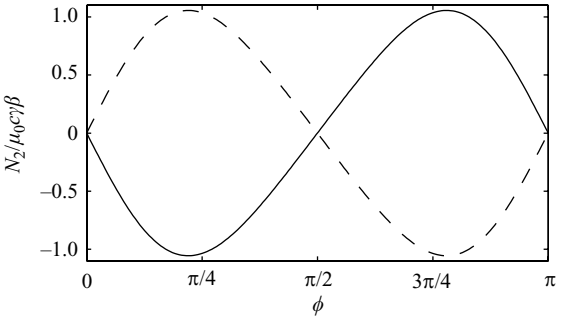

FIGURE 15. Plot of scaled second normal stress difference $N_2/\mu_0 c\dot{\gamma}\beta$ in simple shear flow. The solid line is for a quarter-slipping sphere ($\alpha = \pi/4$); and the broken line is for a three-quarter-slipping sphere ($\alpha = 3\pi/4$).

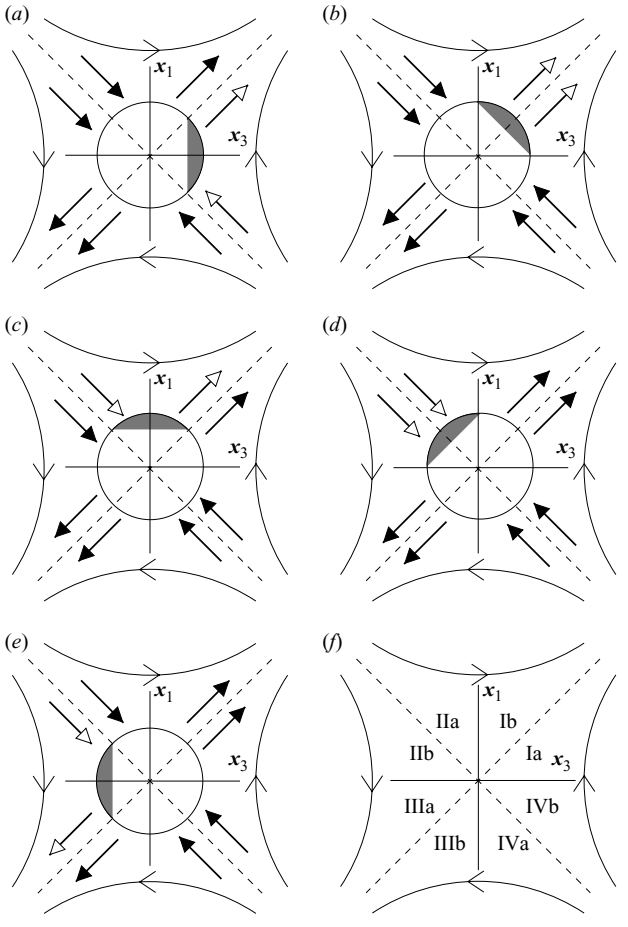

FIGURE 16. Normal stress differences for a quarter-slipping sphere. The legend is the same as in figure 14. When the director is aligned with the velocity or velocity-gradient axes – (*a*), (*c*) and (*e*) – N_1 and N_2 are both zero. However, if the director is aligned with the compressional or extensional axis of the flow – (*b*) and (*d*) – N_2 is non-zero whereas N_1 remains zero.

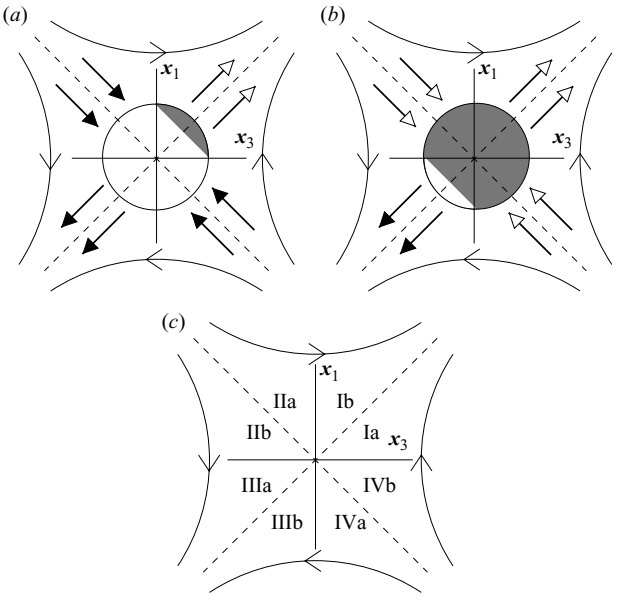

FIGURE 17. Normal stress differences for a quarter-slipping and three-quarter-slipping slip–stick sphere for the equatorial angle $\phi = \pi/4$. The legend is the same as in figure 14.

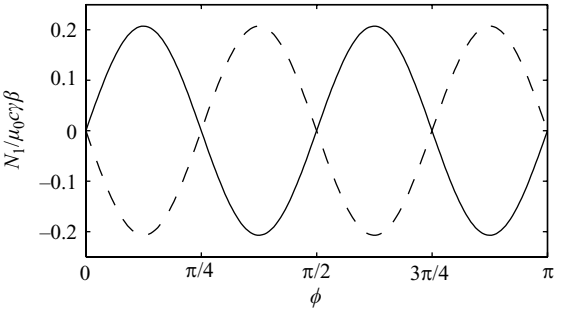

FIGURE 18. Plot of scaled first normal stress difference $N_1/\mu_0 c\dot{\gamma}\beta$ in simple shear flow. The solid line is for a quarter-slipping sphere ($\alpha = \pi/4$); and the broken line is for a three-quarter-slipping sphere ($\alpha = 3\pi/4$).

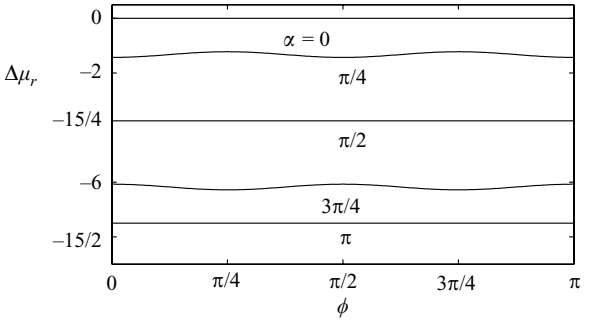

FIGURE 19. Plot of the slipping contribution to the relative viscosity, $\Delta\mu_r = (\mu_r - (1 + 5c/2))/c\beta$, as a function of ϕ for various values of α.

N_2, it is observed that N_1 for a quarter and three-quarter-slipping spheres has opposite signs as a function of ϕ.

Lastly, the dimensionless relative shear viscosity μ_r of the suspension is defined as $\mu_r = \langle \Sigma^P_{13} \rangle / \mu_0 \dot{\gamma}$. Using (4.1) and (4.5) μ_r is given in terms of the g_i functions as

$$\mu_r = 1 + \frac{5}{2}c + c\beta \left(\frac{1}{2} g_1 + (d_1 d_3)^2 g_2 + \frac{1}{2}(d_1^2 + d_3^2) \right) \tag{4.10}$$

$$= 1 + \frac{5}{2}c + c\beta \left(\frac{1}{2} g_1 + \sin^2\theta \cos^2\phi \sin^2\phi g_2 + \frac{1}{2} \sin^2\theta g_3 \right). \tag{4.11}$$

In the above expression, the $1 + (5/2)c$ contribution is, of course, nothing but the relative viscosity for a dilute suspension of no-slip spheres – a result first derived by Einstein (1906). The remaining term, proportional to $c\beta$, represents the effect of slip on the relative viscosity. As the slipping angle increases, the shear stress on the sphere's surface decreases; hence, one expects that μ_r decreases with increasing α. Indeed, this behaviour is observed in figure 19 in which we plot the slip contribution to the relative viscosity, $\Delta\mu_r = (\mu_r - (1 + 5c/2))/c\beta$, as a function of the director orientation ϕ (with $\theta = \pi/2$) for various α. The slipping contribution decreases monotonically from $\Delta\mu_r = 0$ at $\alpha = 0$. For an entirely slipping sphere, we find $\Delta\mu_r = 15/2$, which is in agreement with Happel & Brenner (1965). Interestingly, for a half-slipping sphere, the relative viscosity does not vary with director orientation – the slipping contribution attains a constant value of $\Delta\mu_r = -15/4$.

In the above discussion, we note that the orientational dynamics of the director d_i is determined solely by the imposed flow. For a simple shear flow the director executes a Jeffrey orbit; consequently, the rheology will be periodic in time. A complete analysis of the rheological properties of a dilute suspension of slip–stick spheres would require, however, the inclusion of effects that damp out the cyclical motion of the director and lead to a statistically steady orientational distribution. For submicron colloidal particles, the most likely damping effect is due to rotational Brownian motion. In this case, the motion of the director is no longer deterministic; instead, the probability distribution function for finding the director in a particular orientation satisfies an orientational advection–diffusion equation (see, e.g. Hinch & Leal 1972; Kim & Karrila 2005). This equation reflects a balance between the imposed flow acting to orient the particle and the randomizing influence of Brownian rotation. The ratio of these effects is given by a rotary Péclet number, $Pe = \dot{\gamma}/D_R$ (here D_R is the rotational diffusivity). Moreover, the various contributions to the particle stress in (4.5) must now be weighted by the probability of finding the director in a particular orientation. The rheology of a Brownian suspension of slip–stick spheres will thus share many similarities with that of a suspension of spheroids (Hinch & Leal 1972); however, a detailed analysis is beyond the scope of this work.

5. Conclusions

Almost 20 years ago, Casagrande *et al.* (1989) fabricated the first amphiphilic micron-sized spheres and coined the term 'Janus bead' to describe their dual-faced nature. Two years later, on the occasion of his Nobel lecture, De Gennes (1992) referred to these spheres as 'Janus grains' and commented on their potential application as surfactants with precisely tailored characteristics. These founding works have triggered much interest in fabricating micro- and nanoscale Janus particles with anisotropic chemical, electrical and magnetic properties (Perro *et al.* 2005; Walther

& Muller 2008). More recently, efforts have been focused toward understanding the dynamics of Janus particles with a view to application in microfluidic devices (Howse *et al.* 2007; Gangwal *et al.* 2008). In this paper, we have investigated the dynamics of a hydrodynamically Janus sphere in a linear flow at zero Reynolds number. The motion of this 'slip–stick' sphere in a linear flow is dramatically different from a surface isotropic sphere. For example, in a simple shear flow the particle executes either a periodic translational orbit or undergoes a net displacement in the flow direction, depending on its initial orientation. Moreover, the director of the particle describes a Jeffrey orbit in orientation space. In a pure straining flow, on the other hand, the slip–stick sphere acquires a preferred orientation along either the compressional or extensional axis of the flow, depending on the ratio of slip to no-slip surface areas. Furthermore, the rheology of a dilute suspension of slip–stick spheres is, in general, non-Newtonian with non-zero first and second normal stress differences. For a truly Janus, or half-half ($\alpha = \pi/2$), slip–stick sphere the rotational dynamics are quite trivial – the particle merely rotates with the angular velocity of the ambient field. Also, the rheology is Newtonian with a reduced Einstein viscosity correction. However, note that a half-half slip–stick sphere does move in a simple shear flow.

As mentioned in § 1, we expect hydrodynamically Janus particles to exist in various physical settings. In particular, amphiphilic Janus particles may behave as slip–stick particles with slip lengths potentially of the order of the particle size (Boehnke *et al.* 1999). This should enable the experimental verification of the dynamical and rheological characteristics predicted in this paper. However, we also anticipate that such studies may be hindered by aggregation of the Janus spheres and their accumulation at interfaces. At the very least, nonetheless, we hope that the present work will aid in the understanding of the low-Reynolds-number hydrodynamics of amphiphilic Janus particles.

The authors wish to thank Dr L. G. Leal, Dr D. T. Leighton and Dr T. M. Squires for helpful discussions.

Appendix A

In this appendix, we derive analytical expressions for the scalars in linearity equations (2.5), (2.6) and (4.3), in the limit $\beta = \lambda/a \ll 1$ via a regular perturbation expansion.

We pose a perturbation expansion of the velocity and pressure fields in the small parameter β

$$\begin{aligned} \boldsymbol{u} &= \boldsymbol{u}^{(0)} + \beta \boldsymbol{u}^{(1)} + \beta^2 \boldsymbol{u}^{(2)} + \cdots, \\ p &= p^{(0)} + \beta p^{(1)} + \beta^2 p^{(2)} + \cdots. \end{aligned} \tag{A 1}$$

In the analysis that follows we assume that the director $\boldsymbol{d}$ of the sphere is oriented along the positive x_3 axis (i.e. $d_i = \delta_{i3}$), while the ambient velocity field $\boldsymbol{\omega}^\infty \times \boldsymbol{x} + \boldsymbol{E}^\infty \cdot \boldsymbol{x}$ is arbitrary. Note that this assumption is made only in this appendix, since it renders convenient the computation of the scalars contained in the linearity expressions developed in § 2.

Let us first solve the zeroth-order problem ($\beta = 0$) when the entire surface of the sphere obeys the no-slip condition. The governing equations are Stokes equations (2.1).

$$\mu_0 \nabla^2 \boldsymbol{u}^{(0)} - \nabla p^{(0)} = 0, \quad \text{and} \quad \nabla \cdot \boldsymbol{u}^{(0)} = 0. \tag{A 2}$$

The boundary conditions in (2.2)–(2.4) assume a simple form in the absence of the slipping portion of the sphere.

$$\boldsymbol{u}^{(0)} \to \boldsymbol{\omega}^{\infty} \times \boldsymbol{x} + \boldsymbol{E}^{\infty} \cdot \boldsymbol{x} \quad \text{as} \quad r \to \infty, \tag{A 3a}$$

$$\boldsymbol{u}^{(0)} = \boldsymbol{U} + \boldsymbol{\omega} \times \boldsymbol{x} \quad \text{at} \quad r = a, \tag{A 3b}$$

where $r = \sqrt{\boldsymbol{x} \cdot \boldsymbol{x}}$. The velocity field at the zeroth order is, by linearity, the sum of the separate contributions of the velocity fields resulting from a no-slip sphere translating with a velocity $\boldsymbol{U}$ and rotating with an angular velocity $\boldsymbol{\omega}$ in an ambient linear flow $\boldsymbol{\omega}^{\infty} \times \boldsymbol{x} + \boldsymbol{E}^{\infty} \cdot \boldsymbol{x}$. These individual velocity fields are available in many standard textbooks on fluid mechanics (e.g. Leal 2007), and are combined as follows:

$$\begin{aligned}\boldsymbol{u}^{(0)} = \frac{1}{4}\left(3\frac{a}{r} + \frac{a^3}{r^3}\right)\boldsymbol{U} + \frac{3}{4}\left(\frac{a}{r^3} - \frac{a^3}{r^5}\right)(\boldsymbol{U}\cdot\boldsymbol{x})\,\boldsymbol{x} + \frac{a^3}{r^3}\boldsymbol{\omega}\times\boldsymbol{x} + \left(1 - \frac{a^5}{r^5}\right)\boldsymbol{E}\cdot\boldsymbol{x} \\ -\frac{5}{2}\left(\frac{a^3}{r^5} - \frac{a^5}{r^7}\right)(\boldsymbol{E} : \boldsymbol{x}\boldsymbol{x})\,\boldsymbol{x} + \left(1 - \frac{a^3}{r^3}\right)\frac{1}{2}\boldsymbol{\omega}^{\infty}\times\boldsymbol{x}.\end{aligned} \tag{A 4}$$

The force, torque and stresslet are, to leading order,

$$\begin{aligned}\boldsymbol{F}^{(0)} &= -6\pi\mu_0 a\boldsymbol{U}, \\ \boldsymbol{T}^{(0)} &= -8\pi\mu_0 a^3(\boldsymbol{\omega} - \boldsymbol{\omega}^{\infty}), \\ \boldsymbol{S}^{(0)} &= \frac{20}{3}\pi\mu_0 a^3\boldsymbol{E}^{\infty}.\end{aligned} \tag{A 5}$$

Let us now examine the first effects of slip on the force, torque and stresslet. The governing equations and boundary conditions at $O(\beta)$ are

$$\mu_0\nabla^2\boldsymbol{u}^{(1)} - \nabla p^{(1)} = 0, \quad \text{and} \quad \nabla\cdot\boldsymbol{u}^{(1)} = 0. \tag{A 6}$$

The far-field boundary condition is quite straightforward

$$\boldsymbol{u}^{(1)} \to 0, \quad \text{as} \quad r \to \infty. \tag{A 7}$$

The velocity field on the slip–stick sphere surface may be written as

$$\boldsymbol{u}^{(1)} = 2a\,[1 - H(\theta - \alpha)]\,(\boldsymbol{I} - \boldsymbol{n}\boldsymbol{n})\cdot\boldsymbol{E}^{(0)}\cdot\boldsymbol{n}. \tag{A 8}$$

where

$$\boldsymbol{E}^{(0)} = \frac{1}{2}[\nabla\boldsymbol{u}^{(0)} + (\nabla\boldsymbol{u}^{(0)})^{\mathrm{T}}]. \tag{A 9}$$

Here H is the Heaviside step function and is used to demarcate the slip ($\theta \leqslant \alpha$) and no-slip ($\theta > \alpha$) portions of the sphere.

To solve for the $O(\beta)$ flow we invoke Lamb's general solution for Stokes equations (e.g. Kim & Karrila 2005). Since the disturbance velocity field $\boldsymbol{u}^{(1)}$ is exterior to the sphere and vanishes at infinity, we employ only the decaying spherical harmonics for the velocity and pressure fields

$$p^{(1)} = \sum_{n=1}^{\infty}\mathscr{P}_{-n-1}, \tag{A 10}$$

$$\begin{aligned}\boldsymbol{u}^{(1)} = \sum_{n=1}^{\infty}\left[-\frac{(n-2)r^2}{2\mu_0 n(2n-1)}\nabla\mathscr{P}_{-n-1} + \frac{(n+1)p_{-n-1}\boldsymbol{x}}{\mu_0 n(2n-1)}\right] \\ + \sum_{n=1}^{\infty}\left[\nabla\Phi_{-n-1} + \nabla\times(\boldsymbol{x}\chi_{-n-1})\right],\end{aligned} \tag{A 11}$$

where

$$\mathscr{P}_{-n-1} = r^{-n-1}\sum_{m=0}^{n} P_n^m(\cos\theta)\left(A_{mn}\cos m\phi + \tilde{A}_{mn}\sin m\phi\right),$$
$$\Phi_{-n-1} = r^{-n-1}\sum_{m=0}^{n} P_n^m(\cos\theta)\left(B_{mn}\cos m\phi + \tilde{B}_{mn}\sin m\phi\right), \tag{A 12}$$
$$\chi_{-n-1} = r^{-n-1}\sum_{m=0}^{n} P_n^m(\cos\theta)\left(C_{mn}\cos m\phi + \tilde{C}_{mn}\sin m\phi\right).$$

To implement the boundary conditions, we match the radial velocity, the surface divergence and the surface curl on the sphere surface $r = a$

$$u_r^{(1)} = \sum_{n=1}^{\infty}\frac{(n+1)\,a\mathscr{P}_{-n-1}}{2\mu_0\,(2n-1)} - \frac{(n+1)}{a}\Phi_{-n-1} = 0, \tag{A 13a}$$

$$-2u_r^{(1)} - \frac{1}{\sin\theta}\frac{\partial}{\partial\theta}\left(u_\theta^{(1)}\sin\theta\right) - \frac{1}{\sin\theta}\frac{\partial u_\phi^{(1)}}{\partial\phi}$$
$$= -\frac{1}{\sin\theta}\frac{\partial}{\partial\theta}\left[[1-H(\theta-\alpha)]\,E_{\theta r}^{(0)}\sin\theta\right] - \frac{[1-H(\theta-\alpha)]}{\sin\theta}\frac{\partial E_{\phi r}^{(0)}}{\partial\phi}$$
$$= \sum_{n=1}^{\infty}\frac{-n\,(n+1)\,a\mathscr{P}_{-n-1}}{2\mu_0\,(2n-1)} + \frac{(n+1)\,(n+2)}{a}\Phi_{-n-1}, \tag{A 13b}$$

$$\frac{1}{\sin\theta}\frac{\partial}{\partial\theta}\left(u_\phi^{(1)}\sin\theta\right) - \frac{1}{\sin\theta}\frac{\partial u_\theta^{(1)}}{\partial\phi}$$
$$= \frac{1}{\sin\theta}\frac{\partial}{\partial\theta}\left[\left[1-H(\theta-\alpha)\right]E_{\phi r}^{(0)}\sin\theta\right] - \frac{[1-H(\theta-\alpha)]}{\sin\theta}\frac{\partial E_{\theta r}^{(0)}}{\partial\phi}$$
$$= \sum_{n=1}^{\infty} n\,(n+1)\,\chi_{-n-1}. \tag{A 13c}$$

The surface curl and divergence involve differentiation of the Heaviside step function with respect to the polar angle θ, which results in a Dirac-Delta function at $\theta = \alpha$. It should be noted that this is a non-trivial aspect of using a discontinuous surface velocity field in Lamb's solution.

The force, torque and stresslet on the sphere at this order may be computed from the following simple formulae (Kim & Karrila 2005):

$$\left.\begin{aligned}\boldsymbol{F}^{(1)} &= -4\pi\nabla\left(r^3 p_{-2}\right),\\ \boldsymbol{T}^{(1)} &= -8\pi\mu_0\nabla\left(r^3\chi_{-2}\right),\\ \boldsymbol{S}^{(1)} &= -\frac{2\pi}{3}\nabla\nabla\left(r^5 p_{-3}\right).\end{aligned}\right\} \tag{A 14}$$

It can be shown in a relatively straightforward manner that the evaluation of the force, torque and stresslet involves calculation of the following constants only: A_{01}, A_{11}, $\tilde{A}_{11}$, C_{01}, C_{11}, $\tilde{C}_{11}$, A_{02}, A_{12}, $\tilde{A}_{12}$, A_{22} and $\tilde{A}_{22}$. These constants are computed

by invoking the orthogonality property of spherical harmonics

$$\int_0^{2\pi}\int_0^{\pi} P_{n_1}^{m_1}(\cos\theta)\cos(m_1\phi)\,P_{n_2}^{m_2}(\cos\theta)\cos(m_2\phi)\sin\theta\,\mathrm{d}\theta\,\mathrm{d}\phi$$

$$= \int_0^{2\pi}\int_0^{\pi} P_{n_1}^{m_1}(\cos\theta)\sin(m_1\phi)\,P_{n_2}^{m_2}(\cos\theta)\sin(m_2\phi)\sin\theta\,\mathrm{d}\theta\,\mathrm{d}\phi$$

$$= \frac{2\pi(n_1+m_1)!}{(2n_1+1)!(n_1-m_1)!}\delta_{m_1m_2}\delta_{n_1n_2}, \tag{A 15a}$$

$$\int_0^{2\pi}\int_0^{\pi} P_{n_1}^{m_1}(\cos\theta)\cos(m_1\phi)\,P_{n_2}^{m_2}(\cos\theta)\sin(m_2\phi)\sin\theta\,\mathrm{d}\theta\,\mathrm{d}\phi = 0. \tag{A 15b}$$

Application of the above orthogonality relationships on the boundary conditions yields simultaneous algebraic equations involving the constants, which may be solved to yield the individual constants themselves.

Since the slip–stick sphere is force and torque free, we can write

$$\left.\begin{aligned}\boldsymbol{F}^{(0)}+\beta\boldsymbol{F}^{(1)}=0,\\ \boldsymbol{T}^{(0)}+\beta\boldsymbol{T}^{(1)}=0.\end{aligned}\right\} \tag{A 16}$$

From linearity, we expect that the six equations in (A16) will be simultaneous in the six components (three each) of the sphere's translational and rotational velocities, and can therefore be solved easily to yield $\boldsymbol{U}$ and $\boldsymbol{\omega}$. All the algebraic computations in this paper have been performed using the symbolic toolbox in MATLAB.

We are now in a position to determine the scalars B, f_1, f_2, g_1, g_2 and g_3. The slip–stick sphere is placed in different standard linear flows, and the translational velocity, rotational velocity and the particle stress calculated from (A 14) and (A 16) are compared with the expected results from the linear relations [(2.5), (2.6) and (4.3)] to yield the scalar constants in those equations. Recall that throughout this section, we have chosen the director to be along the x_3 axis. Employing the linear equations in (2.5) and (2.6), the translational and angular velocities of the sphere in this orientation are

$$U_i = a\beta\left(f_1E_{i3}^{\infty}+f_2\delta_{i3}E_{33}^{\infty}\right),\ \omega_i=\omega_i^{\infty}+\beta B\epsilon_{i3k}E_{k3}^{\infty}. \tag{A 17}$$

Consider the slip–stick sphere placed in the simple shear flow $u_3^{\infty}=\dot\gamma x_1$. For this field,

$$E^{\infty}=\frac{\dot\gamma}{2}\left(\delta_{i3}\delta_{j1}+\delta_{i1}\delta_{j3}\right)\quad\text{and}\quad\omega_i^{\infty}=-\frac{1}{2}\dot\gamma\delta_{i2}. \tag{A 18}$$

From linearity relationship (2.5), the angular velocity of the sphere in this orientation is

$$\omega_i=\omega_i^{\infty}+\beta B\epsilon_{i3k}E_{k3}^{\infty}. \tag{A 19}$$

Clearly, $\omega_1=\omega_3=0$, while ω_2 is given by

$$\omega_2=-\frac{\dot\gamma}{2}+\beta B\frac{\dot\gamma}{2}. \tag{A 20}$$

Knowing the form of ω_2 from linearity for this particular orientation of the sphere and the imposed flow, one can compare it to the result from the solution of (A 16) to evaluate B as

$$B=-\frac{15}{16}\sin^2\alpha\cos\alpha. \tag{A 21}$$

In the same (simple shear) flow field, the translational velocity U_i of the sphere is

$$U_i = a\beta\frac{\dot{\gamma}}{2} f_1 \delta_{i1}. \tag{A 22}$$

Again, U_i can be calculated from the perturbation expansion, and this yields f_1 as

$$f_1 = -\frac{5}{8}\sin^2\alpha\left(1+\cos^2\alpha\right). \tag{A 23}$$

To obtain f_2, we place the sphere in the planar extensional flow described by

$$E^{\infty} = \dot{\gamma}\left(\delta_{i1}\delta_{j1} - \delta_{i3}\delta_{j3}\right) \quad \text{and} \quad \omega_i^{\infty} = 0. \tag{A 24}$$

The translational velocity of the sphere in this field is given by

$$U_i = -a\beta\dot{\gamma}\left(f_1 + f_2\right)\delta_{i3}. \tag{A 25}$$

Now, separately, from the solution of (A 16), U_3 is obtained as

$$U_3 = \frac{15}{16} a\beta\dot{\gamma}\sin^4\alpha. \tag{A 26}$$

Therefore, f_2 as determined from (A 23), (A 25) and (A 26) is

$$f_2 = \frac{5}{16}\sin^2\alpha(-5\sin^2\alpha + 4). \tag{A 27}$$

Consider now the expression for the particle stresslet in (4.3)

$$\langle S_{ij}\rangle = \frac{20\pi}{3}\mu_0 a^3 E_{ij}^{\infty} + \frac{4\pi}{3}\mu_0 a^3\beta\left[g_1 E_{ij}^{\infty} + g_2\left(\delta_{i3}\delta_{j3} - \frac{\delta_{ij}}{3}\right)E_{33}^{\infty} + g_3\left(\delta_{i3}E_{j3}^{\infty} + \delta_{j1}E_{i1}^{\infty} - \frac{2\delta_{ij}}{3}\right)E_{33}^{\infty}\right]. \tag{A 28}$$

In the simple shear flow defined in (A 18), the component $\langle S_{13}\rangle$ of the traceless stresslet is given by

$$\langle S_{13}\rangle = \frac{10\pi}{3} a^3\mu_0\dot{\gamma} + \frac{2\pi}{3} a^3\mu_0\dot{\gamma}\beta\left(g_1 + g_3\right). \tag{A 29}$$

This component can be evaluated from the perturbation expansion scheme, resulting in

$$g_1 + g_3 = -\frac{15}{8}(1-\cos\alpha)\left(4\cos^4\alpha + 4\cos^3\alpha - \cos^2\alpha - \cos\alpha + 4\right). \tag{A 30}$$

When subjected to the planar extensional flow defined in (A 24), two more equations containing g_1, g_2 and g_3 may be obtained

$$\begin{aligned}\langle S_{11}\rangle - \langle S_{22}\rangle &= \frac{20\pi}{3} a^3\mu_0\dot{\gamma} + \frac{4\pi}{3} a^3\mu_0\dot{\gamma}\beta g_1, \\ &= -\frac{5}{2}\pi\beta a^3\mu_0\dot{\gamma}(1-\cos\alpha)^2(\cos^3\alpha + 2\cos^2\alpha + 3\cos\alpha + 4) \quad \text{(A 31)} \\ \langle S_{22}\rangle &= \frac{4\pi}{9} a^3\mu_0\dot{\gamma}\beta(g_2 + 2g_3) = -\frac{25}{4}\pi\beta a^3\mu_0\dot{\gamma}\cos\alpha\sin^4\alpha. \end{aligned} \tag{A 32}$$

Solving the three simultaneous equations (A 30)–(A 32) for g_1, g_2 and g_3, we find

$$g_1 = -\frac{15}{8}(1-\cos\alpha)^2\left(\cos^3\alpha + 2\cos^2\alpha + 3\cos\alpha + 4\right), \tag{A 33}$$

$$g_2 = \frac{75}{16}\cos\alpha\sin^2\alpha\left(7\cos^2\alpha - 3\right), \tag{A 34}$$

$$g_3 = -\frac{75}{8}\cos^3\alpha\sin^2\alpha. \tag{A 35}$$

Appendix B

In this appendix, we present the grand resistance matrix for the slip–stick sphere. As described in Kim & Karrila (2005), for a rigid particle placed in a linear ambient field under creeping flow conditions, there exists a linear relationship between the force moments and the flow parameters

$$\begin{pmatrix} \boldsymbol{F} \\ \boldsymbol{T} \\ \boldsymbol{S} \end{pmatrix} = \mu_0 \begin{pmatrix} \boldsymbol{A} & \tilde{\boldsymbol{B}} & \tilde{\boldsymbol{G}} \\ \boldsymbol{B} & \boldsymbol{C} & \tilde{\boldsymbol{H}} \\ \boldsymbol{G} & \boldsymbol{H} & \boldsymbol{M} \end{pmatrix} \begin{pmatrix} \boldsymbol{U}^\infty - \boldsymbol{U} \\ \boldsymbol{\omega}^\infty - \boldsymbol{\omega} \\ \boldsymbol{E}^\infty \end{pmatrix}. \tag{B 1}$$

The square matrix in the above equation is termed as the grand resistance matrix. For an axisymmetric body with a director $\boldsymbol{d}$, the submatrices involved in the grand resistance matrix are

$$A_{ij} = X^A d_i d_j + Y^A(\delta_{ij} - d_i d_j) \tag{B 2}$$

$$B_{ij} = \tilde{B}_{ji} = Y^B \epsilon_{ijk} d_k \tag{B 3}$$

$$C_{ij} = X^C d_i d_j + Y^C(\delta_{ij} - d_i d_j) \tag{B 4}$$

$$G_{ijk} = \tilde{G}_{kij} = X^G(d_i d_j - \tfrac{1}{3}\delta_{ij})d_k + Y^G(d_i\delta_{jk} + d_j\delta_{ik} - 2d_i d_j d_k) \tag{B 5}$$

$$H_{ijk} = \tilde{H}_{kij} = Y^H(\epsilon_{ikl} d_j + \epsilon_{jkl} d_i)d_l \tag{B 6}$$

$$M_{ijkl} = X^M d^{(0)}_{ijkl} + Y^M d^{(1)}_{ijkl} + Z^M d^{(0)}_{ijkl} \tag{B 7}$$

where

$$\left.\begin{aligned} d^{(0)}_{ijkl} &= \tfrac{3}{2}\left(d_i d_j - \tfrac{1}{3}\delta_{ij}\right)\left(d_k d_l - \tfrac{1}{3}\delta_{kl}\right), \\ d^{(1)}_{ijkl} &= \tfrac{1}{2}\left(d_i\delta_{jl}d_k + d_j\delta_{il}d_k + d_i\delta_{jk}d_l + d_j\delta_{ik}d_l - 4d_i d_j d_k d_j\right), \\ d^{(2)}_{ijkl} &= \tfrac{1}{2}\left(\delta_{ik}\delta_{jl} + \delta_{jk}\delta_{il} - \delta_{ij}\delta_{kl} + d_i d_j\delta_{kl} + \delta_{ij}d_k d_l - d_i\delta_{jl}d_k\right. \\ &\quad \left. - d_j\delta_{il}d_k - d_i\delta_{jk}d_l - d_j\delta_{ik}d_l + d_i d_j d_k d_j\right). \end{aligned}\right\} \tag{B 8}$$

Using the method outlined in appendix A, the scalar functions X, Y and Z may be determined to leading order in β as

$$\left.\begin{aligned}
X^A &= 6\pi a\left[1-\frac{\beta}{4}(\cos\alpha+2)(1-\cos\alpha)^2\right]\\
Y^A &= 6\pi a\left[1-\frac{\beta}{8}(1-\cos\alpha)(\cos^2\alpha+\cos\alpha+4)\right]\\
Y^B &= \tfrac{9}{2}\pi\beta a^2\sin^2\alpha\\
X^C &= 8\pi a^3\left[1-\frac{3\beta}{4}(\cos\alpha+2)(1-\cos\alpha)^2\right]\\
Y^C &= 8\pi a^3\left[1-\frac{3\beta}{8}(1-\cos\alpha)(\cos^2\alpha+\cos\alpha+4)\right]\\
X^G &= -\tfrac{45}{8}\pi\beta a^2\sin^4\alpha\\
Y^G &= -\tfrac{15}{8}\pi\beta a^2\sin^2\alpha(1+\cos^2\alpha)\\
Y^H &= -\tfrac{15}{2}\pi\beta a^3\sin^2\alpha\cos\alpha\\
X^M &= \frac{20}{3}\pi a^3\left[1-\frac{3\beta}{4}(3\cos^3\alpha+6\cos^2\alpha+4\cos\alpha+2)(1-\cos\alpha)^2\right]\\
Y^M &= \frac{20}{3}\pi a^3\left[1+\frac{3\beta}{8}(4\cos^4\alpha+4\cos^3\alpha-\cos^2\alpha-\cos\alpha+4)(1-\cos\alpha)\right]\\
Z^M &= \frac{20}{3}\pi a^3\left[1-\frac{3\beta}{8}(\cos^3\alpha+2\cos^2\alpha+3\cos\alpha+4)(1-\cos\alpha)^2\right]
\end{aligned}\right\} \tag{B 9}$$

It is possible to derive all the scalars in table 1 using the above resistance matrices, but we will not show that here. As a quick test, however, we demonstrate that the Bretherton constant obtained from the two methods is consistent. The Bretherton constant as defined in Kim & Karrila 2005 is equal to Y^H/Y^C. To leading order in β, from the above equations, this ratio is $-(15/16)\beta\sin^2\alpha\cos\alpha$, which is identical to βB with B as defined in table 1.

Appendix C

In this appendix, we offer a verification of the analysis used to determine the elements of the grand resistance matrix in Appendix B and the scalar functions in table 1, by employing the Lorentz reciprocal theorem to derive the resistance matrices relating force to translation and rotation.

In the absence of external body forces, the reciprocal theorem states that the velocity fields $\boldsymbol{u}$ and associated stress tensors $\boldsymbol{\sigma}$ for two Stokes flows (labelled $\mathscr{A}$ and $\mathscr{B}$) in the same domain are related via (Happel & Brenner 1965)

$$\int \boldsymbol{u}_{\mathscr{A}}\cdot\boldsymbol{\sigma}_{\mathscr{B}}\cdot\boldsymbol{n}\,\mathrm{d}S = \int \boldsymbol{u}_{\mathscr{B}}\cdot\boldsymbol{\sigma}_{\mathscr{A}}\cdot\boldsymbol{n}\,\mathrm{d}S. \tag{C 1}$$

Here, the domain is taken to be that exterior to a sphere of radius a in an unbounded fluid, and the integrals are over the surface of the sphere, with $\boldsymbol{n}$ the outward pointing unit normal. First, for the $\mathscr{A}$-flow we consider a no-slip sphere translating with velocity $\boldsymbol{U}_{\mathscr{A}}$, for which the traction is simply $\boldsymbol{\sigma}_{\mathscr{A}}\cdot\boldsymbol{n} = -(3\mu_0/2a)\boldsymbol{U}_{\mathscr{A}}$.

Thus, the drag force $\boldsymbol{F}_{\mathscr{B}}$ in the second Stokes flow problem is given by

$$\boldsymbol{F}_{\mathscr{B}} = \frac{3\mu_0}{2a}\int \boldsymbol{u}_{\mathscr{B}}\,\mathrm{d}S. \tag{C 2}$$

For the $\mathscr{B}$-flow, we take a slip–stick sphere translating with velocity $\boldsymbol{U}_{\mathscr{B}}$. On the surface of the sphere the fluid velocity is given by the Navier slip condition,

$$\boldsymbol{u}_{\mathscr{B}} = \boldsymbol{U}_{\mathscr{B}} + 2a\beta\boldsymbol{E}_{\mathscr{B}}\cdot\boldsymbol{n}, \tag{C 3}$$

where $\boldsymbol{E}_{\mathscr{B}}$ is the rate-of-strain tensor in the $\mathscr{B}$-flow. Substituting (C 3) into (C 2) yields

$$\boldsymbol{F}_{\mathscr{B}} = -6\pi\mu_0 a\boldsymbol{U}_{\mathscr{B}} - 3\mu_0\beta\int_{S_2}\boldsymbol{E}_{\mathscr{B}}\cdot\boldsymbol{n}\,\mathrm{d}S, \tag{C 4}$$

where the integral is over the slipping part S_2 of the sphere only (figure 1) . To proceed, we note that the second term on the right-hand side of (C 4) is already an $O(\beta)$ quantity. Therefore, in the integrand one requires $\boldsymbol{E}_{\mathscr{B}}$ to only zeroth order in β, which is simply the rate-of-strain tensor for a *no-slip* sphere translating with velocity $\boldsymbol{U}_{\mathscr{B}}$ (cf. A 4). In this case, on the surface $\boldsymbol{E}_{\mathscr{B}}\cdot\boldsymbol{n} = -(3/4a)(\boldsymbol{I}-\boldsymbol{nn})\cdot\boldsymbol{U}_{\mathscr{B}}$, and after a little algebra we find

$$\int_{S_2}(\boldsymbol{I}-\boldsymbol{nn})\,\mathrm{d}S = \frac{\pi a^2}{3}(4-3\cos\alpha-\cos^3\alpha)\boldsymbol{I} - \pi a^2\cos\alpha\sin^2\alpha\,\boldsymbol{dd}. \tag{C 5}$$

Substituting the above into (C 4) yields

$$\begin{aligned}\frac{\boldsymbol{F}_{\mathscr{B}}}{6\pi\mu_0 a} &= \left[\left(1-\frac{\beta}{8}\left(4-3\cos\alpha-\cos^3\alpha\right)\right)\boldsymbol{I} - \frac{3\beta}{8}\cos\alpha\sin^2\alpha\,\boldsymbol{dd}\right]\cdot\boldsymbol{U}_{\mathscr{B}}\\ &= \left[\left(1-\frac{\beta}{4}(\cos\alpha+2)(1-\cos\alpha)^2\right)\boldsymbol{dd}\right.\\ &\quad\left.+\left(1-\frac{\beta}{8}\left(4-3\cos\alpha-\cos^3\alpha\right)\right)(\boldsymbol{I}-\boldsymbol{dd})\right]\cdot\boldsymbol{U}_{\mathscr{B}},\end{aligned} \tag{C 6}$$

which is exactly the force-translation relation contained in the grand resistance matrix (cf. the functions X^A and Y^A in (B 9)).

Now, to derive the force-rotation coupling, for the $\mathscr{B}$-flow we consider a slip–stick sphere rotating with angular velocity $\boldsymbol{\omega}_{\mathscr{B}}$. On the surface the fluid velocity is

$$\boldsymbol{u}_{\mathscr{B}} = \boldsymbol{\omega}_{\mathscr{B}}\times\boldsymbol{r} + 2a\beta\boldsymbol{E}_{\mathscr{B}}\cdot\boldsymbol{n}. \tag{C 7}$$

Substituting (C 7) into (C 2), we find

$$\boldsymbol{F}_{\mathscr{B}} = -3\mu_0\beta\int_{S_2}\boldsymbol{E}_{\mathscr{B}}\cdot\boldsymbol{n}\,\mathrm{d}S. \tag{C 8}$$

For the reasons explained above, inside the integrand we take $\boldsymbol{E}_{\mathscr{B}}$ as the rate-of-strain tensor of a no-slip sphere rotating with angular velocity $\boldsymbol{\omega}_{\mathscr{B}}$ (cf. A 4). Thus, at $r=a$, $\boldsymbol{E}_{\mathscr{B}}\cdot\boldsymbol{n} = -(3/2)\boldsymbol{\omega}_{\mathscr{B}}\times\boldsymbol{n}$, and

$$\int_{S_2}\boldsymbol{\omega}_{\mathscr{B}}\times\boldsymbol{n}\,\mathrm{d}S = \pi a^2(1-\cos^2\alpha)\boldsymbol{\omega}_{\mathscr{B}}\times\boldsymbol{d}. \tag{C 9}$$

Substituting the above into (C 8) we arrive at the force–rotation relation

$$\boldsymbol{F}_{\mathscr{B}} = \frac{9}{2}\pi\mu_0 a^2\beta(1-\cos^2\alpha)\boldsymbol{\omega}_{\mathscr{B}}\times\boldsymbol{d}, \tag{C 10}$$

as per the resistance function Y^B in (B 9).

Appendix D

In this appendix, we show explicitly that the trace of the particle stress tensor is zero. Consider the stress vector $\boldsymbol{\sigma}\cdot\boldsymbol{n}$ acting on the surface of the sphere ($r=a$) as given by Happel & Brenner (1965)

$$\boldsymbol{\sigma}\cdot\boldsymbol{n}=\frac{\mu_0}{r}\sum_{n=1}^{\infty}\left[-(n+2)\nabla\times(\boldsymbol{x}\chi_{-n-1})-2(n+2)\nabla\Phi_{-n-1}\right.$$
$$\left.-\frac{2n^2-4n+1}{\mu_0 n(2n-1)}\boldsymbol{x}p_{-n-1}+\frac{(n+1)(n-1)}{\mu_0 n(2n-1)}r^2\nabla p_{-n-1}\right]. \tag{D 1}$$

In order to calculate the trace of the force dipole, we require the expression for $\boldsymbol{x}\cdot\boldsymbol{\sigma}\cdot\boldsymbol{n}$ at $r=a$, which may be obtained from the above equation as

$$\boldsymbol{x}\cdot\boldsymbol{\sigma}\cdot\boldsymbol{n}=\frac{\mu_0}{r}\sum_{n=1}^{\infty}\left[-(n+2)\boldsymbol{x}\cdot\nabla\times(\boldsymbol{x}\chi_{-n-1})-2(n+2)\boldsymbol{x}\cdot\nabla\Phi_{-n-1}\right.$$
$$\left.-\frac{2n^2-4n+1}{\mu_0 n(2n-1)}r^2p_{-n-1}+\frac{(n+1)(n-1)}{\mu_0 n(2n-1)}r^2\boldsymbol{x}\cdot\nabla p_{-n-1}\right]. \tag{D 2}$$

Now, since

$$\begin{aligned}\boldsymbol{x}\cdot\nabla\times(\boldsymbol{x}\chi_{-n-1})&=0,\\ \boldsymbol{x}\cdot\nabla\Phi_{-n-1}&=-(n+1)\Phi_{-n-1},\\ \boldsymbol{x}\cdot\nabla p_{-n-1}&=-(n+1)p_{-n-1},\end{aligned} \tag{D 3}$$

(D 2) simplifies to

$$\boldsymbol{x}\cdot\boldsymbol{\sigma}\cdot\boldsymbol{n}=\frac{\mu_0}{a}\sum_{n=1}^{\infty}\left[2(n+1)(n+2)\Phi_{-n-1}-\frac{n^2+3n-4}{\mu_0(2n-1)}a^2p_{-n-1}\right]. \tag{D 4}$$

The trace of the force dipole is, therefore,

$$\int_S\boldsymbol{x}\cdot\boldsymbol{\sigma}\cdot\boldsymbol{n}\,\mathrm{d}S=\frac{\mu_0}{a}\sum_{n=1}^{\infty}\left[2(n+1)(n+2)\int_S\Phi_{-n-1}\mathrm{d}S-\frac{n^2+3n-4}{\mu_0(2n-1)}a^2\int_S p_{-n-1}\mathrm{d}S\right]. \tag{D 5}$$

The two integrals on the right-hand side of the above equation can readily be shown to vanish for $n\geqslant 1$. Hence, the trace of the force dipole is identically zero.

REFERENCES

Basset, A. B. 1961 *A Treatise on Hydrodynamics*. Dover.

Batchelor, G. K. 1970 Stress system in a suspension of force-free particles. *J. Fluid Mech.* **41**, 545–570.

Batchelor, G. K. 1973 *An Introduction to Fluid Dynamics*. Cambridge University Press.

Behrend, C. J., Anker, J. N., McNaughton, B. H., & Kopelman, R. 2005 Microrheology with modulated optical nanoprobes (MOONs). *J. Magn. Magn. Mater.* **293**, 663–670.

Beitel, A. & Heideger, J. W. 1971 Surfactant effects on mass transfer from drops subject to interfacial instability. *Chem. Engng Sci.* **26**, 711–717.

Boehnke, U. C., Remmler, T., Motschmann, H., Wurlitzer, S., Hauwede, J. & Fischer, Th. M. 1999 Partial air wetting on solvophobic surfaces in polar liquids. *J. Colloid Interface Sci.* **211**, 243–251.

Bretherton, F. P. 1962 The motion of rigid particles in a shear flow at low Reynolds number. *J. Fluid Mech.* **14**, 284–304.

Casagrande, C., Fabre, P., Raphael, E. & Veyssie, M. 1989 Janus beads: realization and behaviour at water/oil interfaces. *Europhys. Lett.* **9** (3), 251–255.

Cayre, O., Paunov, V. N. & Velev, O. D. 2003 Fabrication of asymmetrically coated colloid particles by microcontact printing techniques. *J. Mat. Chem.* **13** (10), 2445–2450.

Cheng, J. T. & Giordano, N. 2002 Fluid flow through nanometre-scale channels. *Phys. Rev.* E **65**, 031206.

Choi, C.-H., Westin, K. Johan A. & Breuer K. S. 2003 Apparent slip flows in hydrophilic and hydrophobic microchannels. *Phys. Fluids* **15** (10), 2897–2902.

De Gennes, P. G. 1992 Soft Matter. *Rev. Mod. Phys.* **64**, 645–648.

Dietrich, C., Bagatolli, L. A., Volovyk, Z. N., Thompson, N. L., Levi, M., Jacobson, S. K. & Gratton, E. 2001 Lipid rafts reconstituted in model membranes. *Biophys. J.* **80**, 1417–1428.

Dorrepaal, J. M. 1978 The Stokes resistance of a spherical cap to translational and rotational motions in a linear shear flow. *J. Fluid Mech.* **84**, 265–279.

Einstein, A. 1906 A new determination of molecular dimensions. *Ann. Phys.* **19**, 289–306.

Ericksen, J. L. 1959 Anisotropic fluids. *Arc. Rat. Mech. Anal.* **4**, 231–237.

Gangwal, S., Cayre, O. J., Bazant, M. Z. & Velev, O. D. 2008 Induced-charge electrophoresis of metallodielectric particles. *Phys. Rev. Lett.* **100**, 058302.

Glaser, N., Adams, D. J., Boker, A. & Krausch, G. 2006 Janus particles and liquid–liquid interfaces. *Langmuir* **22**, 5227–5229.

Glotzer, S. C. & Solomon, M. J. 2007 Anisotropy of building blocks and their assembly into complex structures. *Nat. Mater.* **6**, 557–562.

Happel, J. & Brenner, H. 1965 *Low Reynolds Number Hydrodynamics*. Prentice-Hall.

Hinch, E. J. & Leal, L. G. 1972 The effect of Brownian motion on the rheological properties of a suspension of non-spherical particles. *J. Fluid Mech.* **52** (4), 683–712.

Hong, L., Jiang, S. & Granick, S. 2006 Simple method to produce Janus colloidal particles in large quantity. *Langmuir* **22** (23), 9459–9499.

Howse, J. R., Jones, R. A. L., Ryan, A. J., Gough, T., Vafabakhsh, R. & Golestanian, R. 2007 Self-motile colloidal particles: from directed propulsion to random walk. *Phys. Rev. Lett.* **99**, 048102.

Kim, S. & Karrila, S. J. 2005 *Microhydrodynamics: Principles and Selected Applications*. Dover.

Korlach, J., Schwille, P., Webb, W. & Feigenson, G. 1999 Characterization of lipid bilayer phases by confocal microscopy and fluorescence correlation spectroscopy. *Proc. Natl. Acad. Sci.* **96**, 8461–8466.

Lamb, H. 1932 *Hydrodynamics*. Dover.

Lauga, E., Brenner, M. P. & Stone, H. A. 2007 Microfluidics: the no-slip boundary condition. In *Handbook of Experimental Fluid Dynamics* (ed. C. Tropea, A. Yarin & J. F. Foss), pp. 1219–1240. Springer.

Lauga, E. & Stone, H. A. 2003 Effective slip in pressure-driven Stokes flow. *J. Fluid Mech.* **489**, 55–77.

Leal, L. G. 2007 *Advanced Transport Phenomena*. Cambridge University Press.

Navier, C. L. M. H. 1823 Mémoire sur le lois du mouvement des fluides. *Mémoires de l'Academie Royale des Sciences de l'Instituit de France* **IV**, 389–440.

Nie, Z., Li, W., Seo, M., Xu, S. & Kumacheva, E. 2006 Janus and Ternary particles generated by microfluidic synthesis: design, synthesis and self-assembly. *J. Am. Chem. Soc.* **128** (29), 9408–9412.

Nir, A. & Acrivos, A. 1973 On the creeping motion of two arbitrary-sized touching spheres in a linear shear field. *J. Fluid Mech.* **59**, 209–223.

Nisisako, T., Torii, T., Takahashi, T. & Takizawa, Y. 2006 Synthesis of monodisperese bicolored Janus particles with electrical anisotropy using a microfluidic co-flow system. *Adv. Mater.* **18**, 1152–1156.

Perro, A., Reculusa, S., Ravaine, S., Bourgeat-Lami, E. B. & Duguet, E. 2005 Design and synthesis of Janus micro- and nanoparticles. *J. Mat. Chem.* **15**, 3745–3760.

Philip, J. R. 1972*a* Flows satisfying mixed no-slip and no-shear conditions. *Z. Agnew. Math. Phys.* **23**, 353–370.

Philip, J. R. 1972*b* Integral properties of flows satisfying mixed no-slip and no-shear conditions. *Z. Agnew. Math. Phys.* **23**, 960–968.

Priezjev, N. V., Darhuber, A. A. & Troian, S. M. 2005 Slip behaviour in liquid films on surfaces of patterned wettability: comparison between continuum and molecular dynamics simulations. *Phys. Rev.* E **71**, 041608.

Roh, K., Martin, D. C. & Lahann, J. 2005 Biphasic Janus particles with nanoscale anisotropy. *Nat. Mater.* **4**, 759–763.

Sadhal, S. S. & Johnson, R. E. 1983 Stokes flow past bubbles and drops partially coated with thin films. Part 1. Stagnant cap of surfactant film – exact solution. *J. Fluid Mech.* **126**, 237–250.

Squires, T. M. & Bazant, M. Z. 2006 Breaking symmetries in induced-charge electro-osmosis and electrophoresis. *J. Fluid Mech.* **560**, 65–101.

Swan, J. W. & Khair, A. S. 2008 On the hydrodynamics of "slip-stick" spheres. *J. Fluid Mech.* **606**, 115–132.

Takei, H. & Shimizu, N. 1997 Gradient sensitive microscopic probes prepared by gold evaporation and chemisorption on latex spheres. *Langmuir* **13** (7), 1865–1868.

Taylor, G. I. 1971 A model for the boundary condition of a porous material. Part 1. *J. Fluid Mech.* **49**, 319–326.

Thompson, P. A. & Troian, S. M. 1997 A general boundary condition for liquid flow at solid surfaces. *Nature* **389**, 360–362.

Tyrrell, J. W. G. & Attard, P. 2001 Images of nanobubbles on hydrophobic surface and their interactions. *Phys. Rev. Lett.* **87** (17), 176104.

Velev, O. D., Lenhoff, A. M. & Kaler, E. W. 2000 A class of microstructured particles through colloidal crystallization. *Science* **287**, 2240–2243.

Walther, A. & Muller, A. H. E. 2008 Janus particles. *Soft Matter* **4**, 663–668.